Phase field modeling of precipitation and dissolution processes in porous media: Upscaling and numerical experiments

Carina Bringedal, Lars von Wolff, and Iuliu Sorin Pop

UHasselt Computational Mathematics Preprint
Nr. UP-19-01

Jan. 15, 2019

Phase field modeling of precipitation and dissolution processes in porous media: Upscaling and numerical experiments

Carina Bringedal[1,2], Lars von Wolff[3], and Iuliu Sorin Pop[2]

[1]Institute for Modelling Hydraulic and Environmental Systems, University of Stuttgart, Pfaffenwaldring 61, 70569 Stuttgart, Germany
[2]Faculty of Sciences, Hasselt University, Agoralaan Gebouw D, 3590 Diepenbeek, Belgium
[3]Institute of Applied Analysis and Numerical Simulation, University of Stuttgart, Pfaffenwaldring 57, 70569 Stuttgart, Germany
carina.bringedal@iws.uni-stuttgart.de, lars.von-wolff@mathematik.uni-stuttgart.de, sorin.pop@uhasselt.be

15.01.2019

Abstract

We consider a model for precipitation and dissolution in a porous medium, where ions transported by a fluid through the pores can precipitate at the pore walls and form mineral. Also, the mineral can dissolve and become part of the fluid as ions. These processes lead to changes in the flow domain, which are not known a-priori but depend on the concentration of the ions dissolved in the fluid. Such a system can be formulated through conservation equations for mass, momentum and solute in a domain that evolves in time. In this case the fluid and mineral phases are separated by a sharp interface, which also evolves. We consider an alternative approach by introducing a phase field variable, which has a smooth, diffuse transition of non-zero width between the fluid and mineral phases. The evolution of the phase field variable is determined through the Allen-Cahn equation. We show that as the width of the diffuse transition zone approaches zero, the sharp-interface formulation is recovered. Considering a periodically perforated domain mimicking a porous medium, the phase field formulation is upscaled to Darcy scale by homogenization. Then, the average of the phase field variable represents the porosity. Through cell problems, the effective diffusion and permeability matrices are depending on the phase field variable. We consider some numerical examples to show the behavior of the phase field formulation with respect to the width of the diffuse interface, both in the cell problems for a perforated porous medium and for a thin strip.

1 Introduction

Understanding mineral dissolution and precipitation processes in porous media are important as they appear in many applications of highest societal relevance. Examples in this sense are in soil salinization, geological CO2 sequestration, copper leaching or geothermal energy. In many of the situations mentioned above, experiments are unfeasible or even impossible, hence simulations based on reliable and accurate mathematical modeling is a key strategy. The most challenging aspect for the mathematical modeling appears when the flow domain is altered due to dissolution and precipitation. More precisely, the dissolved ions can form a mineral, hence they can leave the fluid domain and rather become part of the stationary mineral domain. Due to this, the space available for flow (the fluid domain) is reduced whereas the mineral domain is increasing. Oppositely, the mineral domain shrinks as minerals dissolve into ions becoming part of the fluid. To mathematically model such processes one needs conservation laws for mass, momentum and solute in time-dependent domains, where the evolution of the interface separating the two domains is not known a-priori. Hence, we have a free boundary problem, where the development of the boundary - and hence also the domains - must be accounted for.

When encountered in a porous medium, mineral precipitation and dissolution can significantly alter the pore structure, and hence affect the porosity and the large-scale flow through the medium as the permeability

evolves. For porous media flow, we separate between two spatial scales. The detailed behavior is found at the pore scale (the micro-scale) and the average behavior of the system is considered at the Darcy scale (the macro-scale). Mineral precipitation and dissolution at the Darcy-scale have been considered from a theoretical point of view by [16], where consistent reaction rates are formulated for the dissolution and precipitation processes, and traveling waves solutions are found. The existence and uniqueness of such solutions are further analyzed in [26]. At the pore scale, the existence of weak solutions is proved in [25], while uniqueness is obtained in [31]. [25] also analyzes the occurrence of dissolution fronts in a thin strip, introducing a free boundary separating regions where mineral is present from those which are mineral-free. In [17], homogenization techniques are employed to prove rigorously that the Darcy-scale model in [16, 26] is the upscaled counterpart of the pore-scale model in [25].

In all cases mentioned above, the mineral layer is assumed to have a negligible thickness when compared even to the micro-scale (the pores) and therefore the presence of a mineral is accounted in form of a concentration. A different approach is adopted in [30], where the mineral layer is assumed to have a non-negligible thickness and therefore precipitation and dissolution can alter the flow domain at the micro-scale. The existence and uniqueness of a weak solution for this free-boundary model is proved, however, in the simplified case of a one-dimensional domain. This situation has extended to the higher dimensional case. In [28] the pore scale model is defined in a two-dimensional thin strip, where a free-boundary model for precipitation and dissolution is included. The Darcy-scale model is derived by transversal averaging. [27] extend this by considering a general porous medium with periodic grains, and a level set formulation is used to account for the presence of the free boundary at the pore scale. These models were later extended to include temperature-dependence for a thin strip [7] and for a periodic porous medium [8], where the effective properties of the latter model was considered further in [10]. Also, the upscaling in transport dominated regimes, leading to models that are similar to Taylor dispersion is performed in [9, 19]. A similar model is considered in [24], but restricted to pore-scale diffusion processes in evolving domains. There a Darcy-scale model is derived, for which the existence of strong solutions is proved up to clogging.

As mentioned above, different approaches are possible when considering free boundary models. One can formulate an explicit equation for the location of the free boundary, through e.g., the width of the mineral phase in a thin strip as in [9, 7, 19, 28, 30]. For more general geometries, a level set formulation has been widely used, as in [8, 24, 27]. Upscaling using homogenization of level-set formulations can be tedious due to the strong coupling between the level set equation and the other model equations, as the asymptotic expansion has to be applied also for the level set and hence for the location of the interface, as done in [8, 24, 27]. However, the upscaled model still relies on solving the pore-scale level set equation, which is quite challenging for the numerical implementation.

An alternative approach for modeling evolving interfaces is through phase fields. A phase field is an approximation of the characteristic function, and hence attains the value 1 in one domain and 0 in the other, but has a smooth, diffuse transition zone of non-zero width across the interface [11, 20]. The evolution of the phase field is through a phase field equation, which can be derived from a minimization of the free energy. Most commonly used are the Allen-Cahn [4] and Cahn-Hilliard [12] equations for evolution of the phase field. While the Cahn-Hilliard equation has the advantage of conserving the phase field parameter, it introduces fourth-order spatial derivatives which can lead to numerical difficulties. For the Allen-Cahn formulation one can prove that the phase field remains bounded by 0 and 1 and thus in the physical regime, as it involves only second-order derivatives. On the other hand, it is generally not conservative, although conservative reformulations for two-phase flow [15] and multi-component systems [21] exist. However, these formulations are globally and not locally conservative. The Allen-Cahn equation allows the interface to evolve due to curvature effects (Gibbs-Thomson effect), which may or may not be desirable from a chemical point of view [23]. We will use an Allen-Cahn equation for our phase field formulation, although curvature effects are not our primary point of interest. We mention that [32] formulated an Allen-Cahn equation for a solid-liquid interface evolving due to solute precipitation and dissolution, where surface curvature effects were removed. However, the model does not include fluid flow.

To introduce a diffuse transition zone, the model equations (i.e. the conservation of mass, momentum and solute) need to be reformulated in the combined domain of fluid and mineral in a consistent manner. The combined domain is then stationary. This reformulated model has to incorporate the boundary conditions of the original model at the evolving interface as part of the model equations. An essential property of a phase field formulation is that the corresponding sharp-interface formulation (i.e., the original model equations and

boundary conditions at the evolving interface) is recovered when the width of the diffuse interface approaches zero [13, 20]. This limit can be investigated using matched asymptotic expansions [11].

Considering mineral precipitation and dissolution, [29] proposed a phase field formulation based on Allen-Cahn for the movement of the liquid-solid interface, but without flow in the fluid phase. Later [22] extended an equivalent formulation of [29] to include two fluid phases - with curvature effects between them - but still without flow. There, the interfaces are moving due to curvature effects. An Allen-Cahn formulation for two-phase Stokes flow with curvature effects on the evolving fluid-fluid interface, but without chemical reactions, was formulated in [1]. Using matched asymptotic expansion techniques, in each of these three papers it is shown that the phase field models reduce to the corresponding sharp-interface models. The aim in this paper is to formulate a phase field model for mineral precipitation and dissolution, in which the flow of a fluid phase transporting the precipitating solute is also taken into account. The model builds on the ones in [22, 29]. Compared to [1], where the moving interface separates two mobile fluid phases, the current moving interface separates a mobile phase (the fluid) and an immobile (mineral) phase. Therefore the formulation in [1] cannot be applied here. In this respect, the present situation is more similar to the melt convection model considered in [5], where the interface between stationary solid and flowing fluid is evolving due to melting. However, [5] did not consider the sharp-interface limit for their phase field formulation.

This paper is organized as follows. In section 2 the phase field formulation is introduced, based on the sharp interface formulation. Next, in section 3 we show that the phase field formulation reduces to the sharp interface formulation when the width of the diffuse interface approaches zero. Then homogenization techniques are applied in section 4 to derive Darcy-scale counterpart of the phase field model proposed here. Finally, section 5 provides some numerical examples. First we study the behaviour of the upscaled model parameters in terms of the diffuse interface parameter, and then the convergence of the homogenization process for a simplified situation, where the model is defined in a thin strip.

2 Formulation of the reactive transport problem

Before introducing the phase field formulation, we formulate first the corresponding sharp interface model including a free boundary. Both models are restricted to the case where only one fluid phase is present, which, in the case of a porous medium, can be seen as a single-phase, fully saturated flow. Moreover, the density and viscosity of the fluid are assumed constant. Furthermore, we only consider a simplified electrochemical system, where the precipitate is formed at the boundaries of the flow domain (the pore walls) and is the product of the reaction between two ions diffusing into and transported by the flowing fluid. If the diffusion coefficients of the two ions is the same, whereas the system is electro-neutral, one can simplify the chemistry by only considering one equation for the solute concentration, as knowing the concentration of one solute and using the electro-neutrality of the system the other concentration is obtained straightforwardly (see [16, 25, 30]).

The models below are given in a dimensional framework. The nondimensionalization is discussed later, in section 4.2.

2.1 Sharp interface formulation

We start with the sharp interface formulation, which motivates later the phase field model. In this case, we let Ω denote the entire domain (the porous medium), which is divided into two disjoint sub-domains: one occupied by the fluid, and another occupied by the mineral. The mineral layer is the result of precipitation and dissolution, and has therefore a variable thickness that is not known a-priori. Hence the domains occupied by the fluid and by the mineral are both time-dependent. Letting $t \geq 0$ stand for the time variable, and denoting by $\Omega_f(t)$ the (time-dependent) fluid domain, the conservation laws for the fluid, its momentum and for the solute are:

$$\nabla \cdot \mathbf{q} = 0 \qquad \text{in } \Omega_f(t), \tag{1a}$$

$$\rho_f \partial_t \mathbf{q} + \rho_f \nabla \cdot (\mathbf{q} \otimes \mathbf{q}) + \nabla p = \mu_f \nabla^2 \mathbf{q} \qquad \text{in } \Omega_f(t), \tag{1b}$$

$$\partial_t u + \nabla \cdot (\mathbf{q} u) = D \nabla^2 u \qquad \text{in } \Omega_f(t). \tag{1c}$$

Here $\mathbf{q}$ is velocity and p is pressure in the fluid, and ρ_f and μ_f are the constant density and viscosity of the fluid. Finally, u is solute concentration and D its diffusivity.

In the mineral domain $\Omega_m(t)$, the mineral is immobile and has a constant concentration u^*, which reduces (1a)–(1c) to

$$\mathbf{q} = \mathbf{0}, \text{ in } \Omega_m(t).$$

In what follows we assume that the concentration in the mineral is always larger than the one in the fluid, namely $u^* > u(x,t)$ for all $t \geq 0$ and $x \in \Omega_f(t)$.

We let $\Gamma(t)$ stand for the free boundary separating $\Omega_f(t)$ and $\Omega_m(t)$. Observe that for any time t one has

$$\Omega = \Omega_f(t) \cup \Omega_m(t) \cup \Gamma(t), \text{ and } \Omega_f(t) \cap \Omega_m(t) = \emptyset.$$

At $\Gamma(t)$, to guarantee the mass balance we adopt the Rankine-Hugoniot boundary conditions for the fluid and for the solute. We assume that the chemistry does not lead to any volume change, which means that one mineral mole takes exactly the same volume as the one occupied in the fluid by the ion moles forming the mineral (see [8, 27]). With this, the conditions at the moving interface are

$$v_n + \gamma\kappa = -\frac{1}{u^*} f(u) \qquad \text{on } \Gamma(t), \tag{2a}$$

$$\mathbf{q} = \mathbf{0} \qquad \text{on } \Gamma(t), \tag{2b}$$

$$v_n(u^* - u) = \mathbf{n} \cdot D\nabla u \qquad \text{on } \Gamma(t), \tag{2c}$$

where v_n is the speed of the moving interface in the normal direction $\mathbf{n}$ pointing into the mineral, γ is the diffusivity of the interface, and κ is the curvature of the moving interface.

Observe that (2a) is describing the movement of the free boundary due to precipitation and dissolution. More precisely, the function f is the difference between the precipitation rate and the dissolution rate. Without being restricted to this choice, we use a simple reaction rate inspired by the mass action kinetics, namely

$$f(u) = f_p(u) - f_d = k\left(\frac{u^2}{u_{\text{eq}}^2} - 1\right), \tag{3}$$

where u_{eq} is the (known) equilibrium concentration for which $u^* > u_{\text{eq}}$, and k is a reaction constant of dimension $\frac{mol}{m^2 \cdot s}$. This choice of reaction rate corresponds to a preicipitation rate increasing with ion concentration and a constant dissolution rate. Note that, to avoid dissolution whenever no mineral is present, in [16, 25] the dissolution rate is given as a multi-valued rate involving the Heaviside graph.

As follows from (2a), next to the precipitation and dissolution, the free boundary is also moving due to surface curvature. The latter effect is more common for two-phase flow, but can also occur for interfaces separating a fluid and solid phase. This assumption is natural when minimizing the surface free energy [2, 23]. In our case, γ will be very small.

The last two conditions at $\Gamma(t)$ are ensuring the mass balance for the fluid and for the solute. Since we assume no volume change in connection with the chemistry, the normal component of the fluid velocity is zero at the moving boundary. Combined with the no-slip condition it follows that the fluid velocity $\mathbf{q}$ is zero at the moving boundary. Finally, (2c) is the Rankine-Hugoniot condition for the ions. The flux on the right-hand side is due to diffusion as the convective flux is zero, following from (2b). Also, the mineral is immobile, so the flux in the mineral sub-domain is 0 whereas the concentration u^* is fixed.

For completeness we mention that the location of the moving interface $\Gamma(t)$ can be determined as the 0 level-set of a function $S : \Omega \times [0, \infty) \to \mathbb{R}$ satisfying

$$S(x,t) = \begin{cases} < 0 & \text{if } x \in \Omega_f(t), \\ 0 & \text{if } x \in \Gamma(t), \\ > 0 & \text{if } x \in \Omega_m(t). \end{cases}$$

Then, S satisfies the equation

$$\partial_t S + v_n |\nabla S| = 0 \text{ for } x \in \Omega.$$

2.2 Phase field formulation

An alternative to the sharp-interface formulation given above is to consider a phase-field formulation. In this case one uses a phase field, which is an approximation of the characteristic function. The non-dimensional phase field ϕ are close to and approaches 1 in the fluid phase, and to 0 in the mineral, and has a smooth transition of (dimensional) width $O(\lambda) > 0$ separating the phases. In other words, $\lambda > 0$ is a phase field parameter related to the thickness of the diffusive transition region. It is to be expected that when passing λ to 0, one obtains in the limit the original sharp-interface model. In consequence, the phase-field approach replaces the interface between the two phases by a smooth transition region where diffusive effects are included. The advantage is that the model equations can now be defined on a stationary domain (here Ω) and not in time-evolving domains. This approach, however, requires the flow and transport equations to also be defined in the mineral phase as well. Here we extend the phase field models in [22, 29] to include flow:

$$\lambda^2 \partial_t \phi + \gamma P'(\phi) = \gamma \lambda^2 \nabla^2 \phi - 4\lambda\phi(1-\phi)\frac{1}{u^*} f(u), \tag{4a}$$

$$\nabla \cdot (\phi \mathbf{q}) = 0, \tag{4b}$$

$$\rho_f \partial_t(\phi \mathbf{q}) + \rho_f \nabla \cdot (\phi \mathbf{q} \otimes \mathbf{q}) = -\phi \nabla p + \mu_f \phi \nabla^2(\phi \mathbf{q}) - g(\phi, \lambda)\mathbf{q} + \frac{1}{2}\rho_f \mathbf{q} \partial_t \phi. \tag{4c}$$

$$\partial_t\big(\phi(u - u^*)\big) + \nabla \cdot (\phi \mathbf{q} u) = D \nabla \cdot (\phi \nabla u). \tag{4d}$$

The model is explained in detail below.

2.2.1 Comments on the phase field equation (4a)

The parameter $\lambda > 0$ appearing in the phase field equation is assumed small and is related to the width of the diffuse interface. Further, $P(\phi) = 8\phi^2(1-\phi)^2$ is the double-well potential, which ensures that the phase field mainly attains values (close to) 0 and 1 for small values of λ. Formally, this follows from the observation that, if λ is small, the term $P'(\phi)$ dominates in (4a), implying that ϕ approaches one of the three equilibrium values $0, 1/2, 1$. Later we show that $1/2$ is an unstable equilibrium, from which the conclusion follows.

The reaction rate $f(u)$ and diffusion parameter γ are the same as in the sharp interface formulation. Note that, due to the $4\phi(1-\phi)$ factor, the reaction term is non-zero only in the diffuse transition zone between the two phases and this factor assures that ϕ stays between 0 and 1. Note that in sharp-interface models, further dissolution after all mineral is dissolved is usually avoided by using a multi-valued dissolution rate based on a Heaviside graph (see [16, 25]), which complicates the analysis and the development of numerical schemes (see [3, 18]). This is superfluous for the phase field formulation proposed here as in the absence of mineral only the water phase is present, implying $\phi = 1$ and therefore no dissolution can take place.

2.2.2 Comments on the flow equations (4b) and (4c)

The flow equations are now also defined in the mineral phase. To ensure that flow only occurs in the fluid and not in the mineral, some modifications have been made: Firstly, the flow velocity $\mathbf{q}$ and pressure gradient ∇p have become $\phi\mathbf{q}$ and $\phi\nabla p$. This leaves the flow equations unchanged in the fluid phase when $\phi = 1$, whereas these quantities are vanishing in the mineral phase where $\phi = 0$.

Secondly, the term $g(\phi, \lambda)\mathbf{q}$ is added. Here, $g(\phi, \lambda)$ is a decreasing, surjective and twice differentiable function fulfilling $g(1, \lambda) = 0$ and $g(0, \lambda) > 0$. This way, $\mathbf{q} = \mathbf{0}$ is the only possible solution when $\phi = 0$ (also see assumption A.4 in [14]). Moreover, this term must also ensure that the velocities in the diffuse transition zone between $\phi = 0$ and $\phi = 1$ are low and therefore works as a interpolation function for velocities in this zone. In [5], dealing with a similar model for melting and solidification, an artificial friction term in introduced to ensure the desired behavior for $\phi\mathbf{q}$ inside the diffuse interface. Using the current notation, their friction term would correspond to $g(\phi, \lambda) = \frac{K(1-\phi)^2\phi}{\lambda^2}$ for some constant K [5]. However, as will be explained in Remark 2, a term of $O(\lambda^{-2})$ would hamper the phase field model to approach the sharp interface model when $\lambda \searrow 0$, and therefore is not adopted here.

A similar idea is adopted in [14], focusing on shape optimization, where the term $g(\phi, \lambda) = \frac{K}{\sqrt{\lambda}}\frac{(1-\phi)n}{\phi+n}$ is applied. The constant $n > 0$ determines the shape of the function g. More precisely, a larger value of n leads to a function that is close to an affine one, behaving as $(1-\phi)$. In [14], $n = 10$ was found to work better regarding

numerical results. Inspired by [14], we let here $g(\phi,\lambda) = \frac{K}{\lambda}\frac{(1-\phi)n}{\phi+n}$ with $n = 10$. Later we will see that this gives good numerical results for the present model too. However, any function g fulfilling the requirements listed previously can be adopted, the specific choice being rather based on the impact on the numerical behavior.

Finally, the term $\frac{1}{2}\rho_f \mathbf{q}\partial_t\phi$ is added to (4c) account for the combined flow with accumulation of the phase field variable, to ensure conservation of kinetic energy when there is precipitation. Note that the two time derivatives can be combined and rewritten to $\rho_f\sqrt{\phi}\partial_t(\sqrt{\phi}\mathbf{q})$, a formulation used in e.g. [6].

2.2.3 Comments on the ion transport equation (4d)

Compared to [22], the only difference appearing in the ion transport equation (4d) is in the presence of the convective term. Note that the time derivative can be rewritten as $\partial_t(\phi u + (1-\phi)u^*)$. This is nothing but the derivative of the ion concentrations u (in the fluid phase) and the mineral concentration u^* (in the mineral phase). Recalling that in the mineral phase there is no diffusive or convective transport, (4d) is nothing but the total mass balance of the species.

2.2.4 Decreasing energy of the phase field formulation

The energy associated with the model (4) is given by

$$E = \frac{1}{2}\rho_f\phi\mathbf{q}^2 + \gamma\lambda^{-1}P(\phi) + \frac{1}{2}\gamma\lambda|\nabla\phi|^2 + \phi F(u),$$

and is the sum of the kinetic energy, the free energy of the phase field, and the energy of the ions. The function $F(u)$ is defined implicitly as a solution to the equation

$$\frac{1}{u^*}f(u) = F(u) - F'(u)u + F'(u)u^*.$$

As $f(u)$ is increasing with u, $F(u)$ is convex for $u < u^*$. Differentiating the above, we get that

$$\partial_t(\phi F(u)) = F'(u)\partial_t\big(\phi(u-u^*)\big) + \frac{1}{u^*}f(u)\partial_t\phi.$$

When considering (4) on a bounded domain Ω with no-slip boundary conditions for $\mathbf{q}$ and zero Neumann boundary conditions for ϕ and u at the boundary $\partial\Omega$, one gets

$$\begin{aligned}\frac{\mathrm{d}}{\mathrm{d}t}\int_\Omega E d\mathbf{x} = \int_\Omega \Big[&-\mu_f\nabla(\phi\mathbf{q}) : \nabla(\phi\mathbf{q}) - g(\phi,\lambda)\mathbf{q}^2 - D\phi F''(u)|\nabla u|^2 \\ &- \lambda^{-1}\big(\nu - \frac{1}{u^*}f(u)\big)\big(\nu - 4\phi(1-\phi)\frac{1}{u^*}f(u)\big)\Big]d\mathbf{x},\end{aligned}$$

where $\nu = \gamma\lambda\nabla^2\phi - \gamma\lambda^{-1}P'(\phi)$. The first three terms on the right hand side describe energy dissipation due to viscosity, friction close to the mineral, and diffusion of ions. The fourth term might be positive and thus lead to an increasing energy. This will be the case if curvature effects (see (2a)) counteract the ion reaction. However, for fixed λ, we get a bounded energy growth as in [22]. Note that the increasing energy is possible due to the factor $4\phi(1-\phi)$ in the reactive term in (4a). Using a multi-valued Heaviside graph for the dissolution rate instead of the $4\phi(1-\phi)$-factor, as commented on in section 2.2.1, would result in a model with decreasing energy, while a regularized Heaviside graph would not. To limit the values of ϕ between 0 and 1 and to ease the following analysis and numerical implementation, we choose to keep the factor $4\phi(1-\phi)$ and not use a Heaviside graph.

2.3 Regularized phase field formulation

The model (4) is formulated in the full domain Ω. In doing so, the term $g(\phi,\lambda)\mathbf{q}$ is included to ensure that $\mathbf{q} = \mathbf{0}$ in the mineral phase. Observe that the ion concentration u and the fluid pressure p are also defined in the region occupied by the mineral in the sharp interface formulation. For u, a possible extension in the mineral domain is u^*, but this may lead to difficulties related to the regularity of u in the transition from the phase field model to the sharp interface one, when $\lambda \to 0$. Moreover, there is no indication about how to extend p in

the mineral domain. At the same time, the model in (4) does not provide any information about what values u and p should attain in the mineral domain. Although the structure of the phase field equation (4a) assures that ϕ will never reach 0 (nor 1), unless initialized so or if appearing on the boundary $\partial\Omega$, ϕ can become arbitrarily close to 0 (and 1). From a numerical point of view, this can lead to a badly conditioned discretization, as the last two equations in (4) are close to degenerate whenever $\phi \searrow 0$ and cannot be used to determine u and p in the mineral. To avoid this, we regularize the model by adding a small, non-dimensional $\delta > 0$ to the phase field ϕ in the mass, momentum and solute conservation equations. The regularized model becomes

$$\lambda^2 \partial_t \phi + \gamma P'(\phi) = \gamma \lambda^2 \nabla^2 \phi - 4\lambda\phi(1-\phi)\frac{1}{u^*} f(u), \tag{5a}$$

$$\nabla \cdot \big((\phi+\delta)\mathbf{q}\big) = 0, \tag{5b}$$

$$\begin{aligned}\rho_f \partial_t \big((\phi+\delta)\mathbf{q}\big) + \rho_f \nabla \cdot \big((\phi+\delta)\mathbf{q}\otimes\mathbf{q}\big) &= -(\phi+\delta)\nabla p \\ &+\mu_f(\phi+\delta)\nabla^2\big((\phi+\delta)\mathbf{q}\big) - g(\phi,\lambda)\mathbf{q} + \frac{1}{2}\rho_f \mathbf{q}\partial_t\phi,\end{aligned} \tag{5c}$$

$$\partial_t\big((\phi+\delta)(u-u^*)\big) + \nabla\cdot\big((\phi+\delta)\mathbf{q}u\big) = D\nabla\cdot\big((\phi+\delta)\nabla u\big), \tag{5d}$$

Note that this regularization is only needed to facilitate the numerical discretization. However, for completeness we use it also in the analysis given below.

Remark 1. *The results for decreasing and limited growth of the free energy discussed in section 2.2.4 are also valid for the regularized formulation. To see this, one only needs to replace ϕ by $\phi+\delta$ in the terms associated with the kinetic energy and the energy of the ions.*

3 The sharp interface limit of the phase field formulation

As stated before, the phase field model can be seen as an approximation of the sharp interface model, defined in the entire domain and where the free boundary is replaced by a diffuse interface region. To justify this, we investigate the limit of the phase field model in (5) as λ, the width of the diffuse transition zone, approaches zero and show that this limit is exactly the model in section 2.1 We follow the ideas of [11] and distinguish between the behavior of the solution close to the interface and far away from it. To this aim we first let L be a typical length in the model and introduce the new, dimensionless parameter $\xi = \lambda/L$ related to thickness of the diffuse interface region. We investigate the behavior of the solution as $\xi \searrow 0$ by expanding the unknowns in terms of ξ and equating terms of similar order. This is done in two different ways, close to the diffuse interface (the inner expansions) and away from it (the outer expansions), which are connected by applying matching conditions in the transition region where both expansions are valid.

Before proceeding we mention that for the phase field equation the steps are the same as in [22] and therefore these are only shown briefly. Throughout this matched asymptotic analysis we take the regularization parameter as $\delta = \xi$.

3.1 The two expansions and matching conditions

Away from the interface, we consider the *outer expansion* of ϕ, u, p and $\mathbf{q}$. For ϕ this reads

$$\phi^{\text{out}}(t,\mathbf{x}) = \phi_0^{\text{out}}(t,\mathbf{x}) + \xi\phi_1^{\text{out}}(t,\mathbf{x}) + \xi^2\phi_2^{\text{out}}(t,\mathbf{x}) + \dots, \tag{6}$$

and similarly for the other unknowns.

For the *inner expansion*, valid near the diffuse interface, we switch to local coordinates. More precisely, we let $\Gamma(t)$ denote the set of points $\mathbf{y}_\xi \in \Omega$ along which $\phi(\mathbf{y}_\xi, t) = 1/2$. Observe that these points depend on t, and of ξ as the model depends on $\lambda = L\xi$. With $\mathbf{s}$ being the parameterization along $\Gamma_\xi(t)$ ($\mathbf{s}$ being a scalar in the two-dimensional case) and $\mathbf{n}_\xi$ the normal vector at $\Gamma_\xi(t)$ pointing into the mineral, one can define r, the signed distance from a point $\mathbf{x}$ near $\Gamma_\xi(t)$ to this interface. Clearly, r depends on $\mathbf{x}$ and on t, and is positive in the mineral region. One gets

$$\mathbf{x} = \mathbf{y}_\xi(t,\mathbf{s}) + r\mathbf{n}_\xi(t,\mathbf{s}), \tag{7}$$

as presented in Figure 1. It can be shown (see [11]) that

$$|\nabla r| = 1, \quad \nabla r \cdot \nabla s_i = 0, \quad \partial_t r = -v_n, \quad \nabla^2 r = \frac{\kappa + 2\Pi r}{1 + \kappa r + \Pi r^2},$$

where κ and Π are the mean and Gaussian curvature of the interface. Further, the point $\mathbf{y}_\xi$ has the expansion $\mathbf{y}_\xi = \mathbf{y}_0 + \xi \mathbf{y}_1 + \dots$, where $\mathbf{y}_0$ is a point on the interface $\Gamma_0^{\text{out}}(t)$ defined through $\phi_0^{\text{out}} = 1/2$, and similarly $\mathbf{n}_\xi = \mathbf{n}_0 + \xi\gamma_1 \mathbf{n}_1 + O(\xi^2)$, where $\mathbf{n}_0$ is the normal vector of $\Gamma_0^{\text{out}}(t)$.

With $z = r/\xi$ and in terms of z and $\mathbf{s}$, we consider the *inner expansions*

$$\phi^{\text{in}}(t, \mathbf{x}) = \phi_0^{\text{in}}(t, z, \mathbf{s}) + \xi \phi_1^{\text{in}}(t, z, \mathbf{s}) + \xi^2 \phi_2^{\text{in}}(t, z, \mathbf{s}) + \dots, \tag{8}$$

and similarly for the other unknowns. In the curvilinear coordinates (7), by the scaling of the z variable, the derivatives are rewritten as follows. For a generic variable v or $\mathbf{v}$, we obtain [11]:

$$\begin{aligned}
\partial_t v &= -\xi^{-1} v_{n,0} \partial_z v^{\text{in}} + (\partial_t + \partial_t s \cdot \nabla_{\mathbf{s}}) v^{\text{in}} + O(\xi), \\
\nabla_x v &= \xi^{-1} \partial_z v^{\text{in}} \mathbf{n}_0 + \nabla_\Gamma v^{\text{in}} + O(\xi), \\
\nabla_x \cdot \mathbf{v} &= \xi^{-1} \partial_z \mathbf{v}^{\text{in}} \cdot \mathbf{n}_0 + \nabla_\Gamma \cdot \mathbf{v}^{\text{in}} + O(\xi), \\
\nabla_x^2 v &= \xi^{-2} \partial_{zz} v + \xi^{-1} \kappa_0 \partial_z v + O(1),
\end{aligned}$$

where we have used $\nabla_x^2 r = \kappa_0 + O(\xi)$ is the lowest order mean curvature and $v_n = v_{n,0} + O(\xi)$. Here, κ_0 and $v_{n,0}$ are the curvature and normal velocity of the interface $\Gamma_0^{\text{out}}(t)$. Further, in the last equality, the properties $|\nabla r| = 1$ and $\nabla r \cdot \nabla s_i = 0$ have been used.

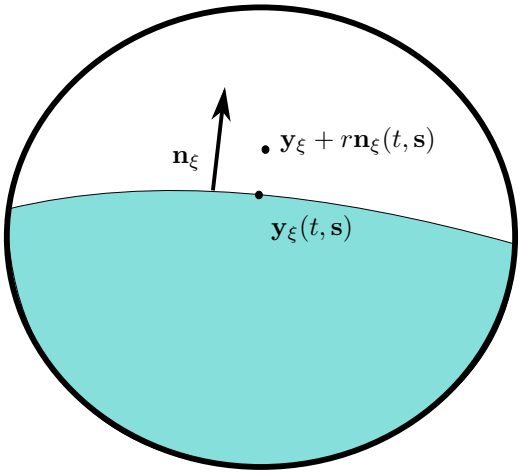

Figure 1: Local coordinates near the interface.

For the outer expansion and a fixed t and $\mathbf{s}$ we let $\mathbf{y}_{1/2\pm}$ denote the limit $r \searrow 0$ (i.e. from the mineral side), respectively $r \nearrow 0$ (from the fluid side) of $\mathbf{x}$ rewritten in terms of the local coordinates in (7). We associate the corresponding limit values of the outer expansion with the ones for the inner expansion, obtained when $z \to \pm\infty$. More precisely, we assume that the two expansions of the phase field ϕ fulfill the following matching conditions [11]:

$$\lim_{z \to \pm\infty} \phi_0^{\text{in}}(t, z, \mathbf{s}) = \phi_0^{\text{out}}(t, \mathbf{y}_{1/2\pm}), \tag{9a}$$

$$\lim_{z \to \pm\infty} \partial_z \phi_0^{\text{in}}(t, z, \mathbf{s}) = 0, \tag{9b}$$

$$\lim_{z \to \pm\infty} \left(\phi_1^{\text{in}}(t, z, \mathbf{s}) - (z + y_1) \nabla \phi_0^{\text{out}}(t, \mathbf{y}_{1/2\pm}) \cdot \mathbf{n}_0 \right) = \phi_1^{\text{out}}(t, \mathbf{y}_{1/2\pm}), \tag{9c}$$

$$\lim_{z \to \pm\infty} \partial_z \phi_1^{\text{in}}(t, z, \mathbf{s}) = \nabla \phi_0^{\text{out}}(t, \mathbf{y}_{1/2\pm}) \cdot \mathbf{n}_0, \tag{9d}$$

and similarly for the other unknowns.

3.2 Outer expansions

Following the steps in [22], we substitute the outer expansion (6) for ϕ into the phase field equation (5a). For the $O(1)$ term, which is the leading order, one obtains

$$P'(\phi_0^{\text{out}}) = 0.$$

This equation has three solutions: $\phi_0^{\text{out}} = 0,\ 1/2$, or 1. Using the formal argument in [29], the first and the last solution are stable since $P''(0)$ and $P''(1)$ are positive, whereas $\phi_0^{\text{out}} = 1/2$ is unstable since $P''(1/2) < 0$. In view of this, we see that in the limit $\xi \to 0$ one obtains the solutions $\phi_0^{\text{out}} = 0$ and $\phi_0^{\text{out}} = 1$, and let $\Omega_0^f(t)$ and $\Omega_0^m(t)$ be the (time dependent) sub-domains of Ω where ϕ_0^{out} is 1 and 0, respectively.

Using the outer expansions in the flow equations (5b) and (5c) and the ion conservation (5d), it is straightforward to show that the original sharp interface model equations (1) are recovered for the points in $\Omega_0^f(t)$. Moreover, for the flow equations one also obtains $\mathbf{q}_0^{\text{out}} = \mathbf{0}$ in $\Omega_0^m(t)$.

3.3 Inner expansions

We now apply the inner expansions and the matching conditions to the phase field model to recover the boundary conditions at the evolving interface.

3.3.1 Phase field equation

For the phase field equation (5a) we follow the steps in [22] and obtain that the dominating $O(1)$ terms satisfy

$$P'(\phi_0^{\text{in}}) = L^2 \partial_z^2 \phi_0^{\text{in}}. \tag{10}$$

Due to (9), one has $\lim_{z\to-\infty} = \phi_0^{\text{in}}(t, z, \mathbf{s}) = 1$ and $\lim_{z\to\infty} \phi_0^{\text{in}}(t, z, \mathbf{s}) = 0$. Further, $\phi_0^{\text{in}}(t, 0, \mathbf{s}) = 0.5$ as this should define the moving interface when $\xi \to 0$. Hence, multiplying (10) by $\partial_z^2 \phi_0^{\text{in}}$, integrating the result in z and using the matching conditions fulfilled by ϕ_0^{in} and the specific form of $P(\phi)$, one gets

$$\partial_z \phi_0^{\text{in}} = -\frac{4}{L} \phi_0^{\text{in}} (1 - \phi_0^{\text{in}}). \tag{11}$$

Since $\phi_0^{\text{in}}(t, 0, \mathbf{s}) = 1/2$, the solution is

$$\phi_0^{\text{in}}(t, z, \mathbf{s}) = \phi_0^{\text{in}}(z) = \frac{1}{1 + e^{4z/L}} = \frac{1}{2}(1 + \tanh(\frac{2z}{L})). \tag{12}$$

For the $O(\xi)$ terms one obtains

$$\big(P''(\phi_0^{\text{in}}) - L^2 \partial_z^2\big)\phi_1^{\text{in}} = (L^2 v_{n,0} + L^2 \gamma \kappa_0)\partial_z \phi_0^{\text{in}} - 4L \phi_0^{\text{in}}(1 - \phi_0^{\text{in}}) \frac{1}{u^*} f(u_0^{\text{in}}).$$

We view the left-hand side as an operator $\mathcal{L}$ depending on ϕ_0^{in} and applied to ϕ_1^{in}. As $\mathcal{L}$ is a Fredholm operator of index zero, the above equation has a solution if and only if the right-hand side, denoted by $A(\phi_0^{\text{in}})$, is orthogonal to the kernel of $\mathcal{L}$. As follows from (10), $\partial_z \phi_0^{\text{in}}$ lies in the kernel of $\mathcal{L}$. Since $v_{n,0}$, κ_0 and u_0^{in} are independent of z (the latter will be shown in the following section), the solvability condition implies

$$\begin{aligned} 0 &= \int_{-\infty}^{\infty} A(\phi_0^{\text{in}}) \partial_z \phi_0^{\text{in}} dz \\ &= L^2 (v_{n,0} + \gamma \kappa_0) \int_{-\infty}^{\infty} (\partial_z \phi_0^{\text{in}})^2 dz - 4L \frac{1}{u^*} f(u_0^{\text{in}}) \int_{-\infty}^{\infty} \phi_0^{\text{in}}(1 - \phi_0^{\text{in}}) \partial_z \phi_0^{\text{in}} dz \\ &= \frac{2}{3} L (v_{n,0} + \gamma \kappa_0 + \frac{1}{u^*} f(u_0^{\text{in}})). \end{aligned}$$

From this, applying matching conditions for u at the moving interface we obtain the condition

$$v_{n,0} = -\gamma \kappa_0 - \frac{1}{u^*} f(u_0^{\text{out}}(t, \mathbf{y}_{1/2-})),$$

which is the first boundary condition (2a) at the moving interface.

3.3.2 Mass conservation equation

The dominating $O(\xi^{-1})$ term arising from inserting the inner expansions into (5b) is

$$\partial_z(\phi_0^{\text{in}}\mathbf{q}_0^{\text{in}})\cdot\mathbf{n}_0 = 0. \tag{13}$$

By integrating with respect to z and using matching conditions, we obtain

$$\mathbf{q}_0^{\text{out}}(t,\mathbf{y}_{1/2-})\cdot\mathbf{n}_0 = 0.$$

In other words, the normal component of the velocity is zero at the moving interface. To conclude the same for the tangential component, we consider the momentum conservation equation.

3.3.3 Momentum conservation equation

The dominating $O(\xi^{-2})$ term in the momentum equation (5c) is

$$\mu_f\phi_0^{\text{in}}\partial_z^2(\phi_0^{\text{in}}\mathbf{q}_0^{\text{in}}) = \mathbf{0}.$$

Integrating with respect to z and using matching conditions results in

$$\mathbf{q}_0^{\text{out}}(t,\mathbf{y}_{1/2-}) = \mathbf{0},$$

which is the second boundary condition (2b) at the moving interface.

Remark 2. *Note that choosing $g(\phi,\lambda) = \frac{K\phi(1-\phi)^2}{\lambda^2}$ as in [5], would lead to the dominating $O(\xi^{-2})$ terms being*

$$\mu_f\phi_0^{in}\partial_z^2(\phi_0^{in}\mathbf{q}_0^{in}) = K\phi_0^{in}(1-\phi_0^{in})^2\mathbf{q}_0^{in}$$

Although μ_f and K are constants, and ϕ_0^{in} is known through (12), solving this equation for $\mathbf{q}_0^{in}$ is not straightforward and therefore it is unclear whether $\mathbf{q}_0^{out}(t,\mathbf{y}_{1/2-}) = \mathbf{0}$ is recovered in this case.

3.3.4 Ion conservation equation

The dominating $O(\xi^{-2})$ term obtained by inserting the inner expansions into (5d) is

$$\partial_z(\phi_0^{\text{in}}\partial_z u_0^{\text{in}}) = 0.$$

Integrating with respect to z and using matching conditions and the fact that $\phi_0^{\text{in}} > 0$, we obtain

$$\partial_z u_0^{\text{in}} = 0,$$

hence $u_0^{\text{in}} = u_0^{\text{in}}(t,\mathbf{s})$ as mentioned in the previous section.

Taking advantage of $\partial_z u_0^{\text{in}} = 0$ and of (13), the $O(\xi^{-1})$ terms satisfy

$$-v_{n,0}(u_0^{\text{in}} - u^*)\partial_z\phi_0^{\text{in}} = D\partial_z(\phi_0^{\text{in}}\partial_z u_1^{\text{in}}).$$

Integrating with respect to z from $-\infty$ to $+\infty$ and applying matching conditions, lead to

$$v_{n,0}(u_0^{\text{out}}(t,\mathbf{y}_{1/2-}) - u^*) = -D\nabla u_0^{\text{out}}(t,\mathbf{y}_{1/2-})\cdot\mathbf{n}_0,$$

which is the third boundary condition (2c) at the moving interface.

4 Upscaling using periodic homogenization

We now consider the phase field model (5) to be defined in a periodic porous medium. The pore scale, where grain, mineral and fluid-filled void space are explicitly separated, will be the micro scale, and we will in the following derive a macro scale model describing the effective behavior of the system. More precisely, we consider a domain $\mathcal{D}$ containing small, periodically distributed grains, as sketched in Figure 2. In a porous medium, $\mathcal{D}$ represent the union of the void space, mineral space and the grain space, where the grains will be considered as perforations. We will refer to the union of the void space and mineral space as the pore space. The grains are impermeable for fluid and no reactions take place there. Hence, the phase field model (5) is not defined in the grain space but only in the pore space of $\mathcal{D}$. The grains do not change with time, while the moving boundary between mineral and fluid, located in the pore space of $\mathcal{D}$, is still handled by the phase field equation as a diffuse interface. We assume that the mineral precipitates on the boundary of the perforations or at already existing minerals, and not inside the void space. Another important assumption is that the void space in $\mathcal{D}$ is connected and that the mineral never grows in such a way that the pore space is clogged.

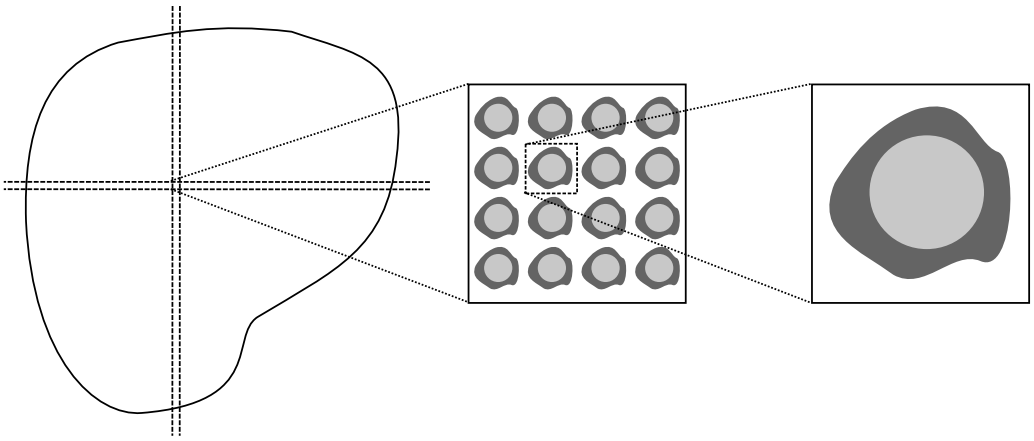

Figure 2: Structure of porous medium. Fluid-filled void space is marked with white, mineral is dark grey, and non-reactive grain is light grey. The pore space is the union of the void space and mineral space.

The porous medium $\mathcal{D}$ contains many periodically repeating grains. This means that the phase field model (5) is defined on a domain of high complexity. In such cases, the averaged behavior of the system is of primary interest. In consequence we apply periodic homogenization techniques to find effective equations valid at a larger scale, where the micro scale oscillations are no longer visible, but their effect is still taken into account. This is done by identifying a scale separation and applying asymptotic expansions on non-dimensional versions of the model equations.

4.1 The scale separation

In the dimensional setting we let ℓ be a typical length scale at the micro scale (that is, the pore scale), e.g., the width of the right-most box in Figure 2) and L a typical length scale at the macro scale, e.g. the width of the domain $\mathcal{D}$. With this we define $\varepsilon = \ell/L$, reflecting the ratio between the micro and macro scales. We assume that ℓ is much smaller than L, hence ε is a small number.

In what follows we rewrite the model in non-dimensional form. In doing so we introduce a local unit cell $Y = [0,1]^{\mathrm{dim}}$, as seen in Figure 3, where dim is 2 or 3, depending on spatial dimension, and we let the local variable $\mathbf{y} \in (0,1)^{\mathrm{dim}}$ describe points within Y. The local cell consists of the fluid part F and mineral part M, and the grain part G as sketched in Figure 3. Hence, locally the phase field model is defined in the pore space $P = F \cup M$, while G defines the perforation. The boundary Γ_P defines the (stationary) internal boundary between perforation and the domain for the phase field model. The boundary ∂Y denotes the outer boundary of the unit cell Y. At this boundary we will later apply periodic boundary conditions allowing to decouple the unit cells from each other. However, when referring to internal boundaries, the boundary Γ_P is meant.

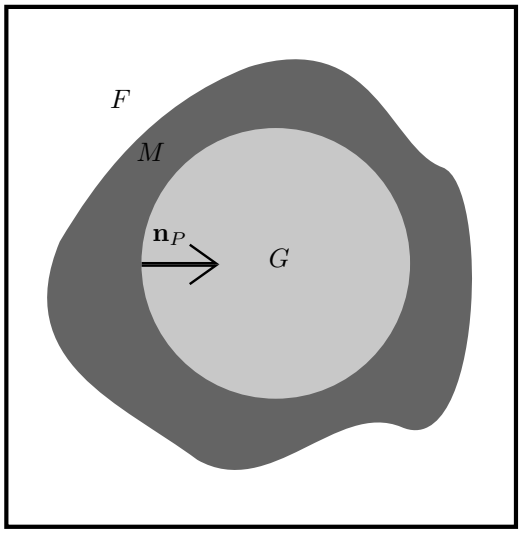

Figure 3: Local pore $Y = [0,1]^d$. The fluid part (white) is F, mineral part (dark grey) is M and grain part (light grey) is G, along with a normal vector $\mathbf{n}_P$ at the internal boundary Γ_P. The outer boundary of the local pore, ∂Y, is marked with black.

To distinguish between the two scales in the model we use $\mathbf{x}$ as the variable at the macro scale, which is then connected to the local, micro scale variable $\mathbf{y}$ through $\mathbf{y} = \varepsilon^{-1}\mathbf{x}$. This can be interpreted as $\mathbf{x}$ only seeing the macro-scale behavior, while the zoomed-in $\mathbf{y}$ sees the micro-scale rapid changes in a single cell. Hence for each macro-scale point $\mathbf{x}$, we can identify a unit cell, with its own local variable $\mathbf{y}$.

With this we have that the perforated domain of the phase field model is the union of all the local pores P, scaled by ε. This means that the domain depends on ε and can be written as

$$\Omega^\varepsilon = \cup_{w\in W_\mathcal{D}}\{\varepsilon(w+P)\},$$

where $W_\mathcal{D}$ is a subset of $\mathbb{Z}^{\dim}$ satisfying $\mathcal{D} = \cup_{w\in W_\mathcal{D}}\{\varepsilon(w+Y)\}$, which is the complete (non-perforated) medium domain seen to the left in Figure 2. We use ε as a superscript to indicate dependence on ε. The union of all internal boundaries Γ_P is denoted by

$$\Gamma^\varepsilon = \cup_{w\in W_\mathcal{D}}\{\varepsilon(w+\Gamma_P)\}.$$

4.2 Non-dimensional model equations

For identifying which terms are dominating in the model and hence are important for the upscaling, we first non-dimensionalize the model equations (5). The assumptions made below on the typical flow rate, viscosity and pressure difference, ensure that we are in the range of Darcy's law, which means that at the macro scale the conservation of momentum equation (5c) becomes a Darcy-like law. Also, we ensure that the diffuse interface (that is, the transition between mineral and fluid) stays within a local pore. Non-dimensional variables and quantities are denoted with a hat and are defined as

$$\begin{aligned}
&\hat{t} = t/t_{\text{ref}}, && \hat{\mathbf{x}} = \mathbf{x}/L, && \hat{\mathbf{y}} = \mathbf{y}/\ell, && \hat{\lambda} = \lambda/\ell,\\
&\hat{\mathbf{q}}^\varepsilon = \mathbf{q}/q_{\text{ref}}, && \hat{u}^\varepsilon = u/u_{\text{ref}}, && \hat{p}^\varepsilon = p/p_{\text{ref}}, && \hat{u}^* = u^*/u_{\text{ref}},\\
&\hat{D} = D/D_{\text{ref}}, && \hat{\mu}_f = \mu_f/\mu_{\text{ref}}, && \hat{\rho}_f = \rho_f/\rho_{\text{ref}} && \hat{k} = k/k_{\text{ref}},\\
& && \hat{\gamma} = \gamma/\gamma_{\text{ref}} && \hat{K} = K/K_{\text{ref}}. &&
\end{aligned}$$

Note the superscript ε for the variables having a highly oscillatory behavior. We assume that the reference quantities are related by

$$\begin{aligned}
&q_{\text{ref}} = L/t_{\text{ref}}, && p_{\text{ref}} = q_{\text{ref}}^2\rho_{\text{ref}}L^2/\ell^2, && D_{\text{ref}} = L^2/t_{\text{ref}}, && \mu_{\text{ref}} = \rho_{\text{ref}}Lq_{\text{ref}}\\
&k_{\text{ref}} = u_{\text{ref}}\ell/t_{\text{ref}}, && \gamma_{\text{ref}} = \ell^2/t_{\text{ref}}, && K_{\text{ref}} = \rho_{\text{ref}}q_{\text{ref}}L/\ell. &&
\end{aligned}$$

The above choices imply that the time scales for transport, diffusion and precipitation and dissolution are comparable, which corresponds to a regime where the Pèclet, Reynolds and Damköhler numbers are of $O(\varepsilon^0)$, and ensure we are in the range of Darcy's law. Further, the scaling of γ_{ref} together with the scaling of λ with ℓ correspond to a Cahn number of $O(\varepsilon)$ which is needed to keep the diffuse transition zone within a local pore. Similarly, the choice of K_{ref} is made to still ensure low velocities in the diffuse transition zone. With the choice of k_{ref}, the non-dimensional reaction rate is given by $\hat{f}(\hat{u}) = \hat{k}(\hat{u}^2/\hat{u}_{\text{eq}}^2 - 1)$.

Since from now on we will only use non-dimensional variables, we skip the hat on all variables. With this, the dimensionless model reads

$$\lambda^2 \partial_t \phi^\varepsilon + \gamma P'(\phi^\varepsilon) = \varepsilon^2 \gamma \lambda^2 \nabla^2 \phi^\varepsilon - 4\lambda \phi^\varepsilon (1-\phi^\varepsilon) \frac{1}{u^*} f(u^\varepsilon) \qquad \text{in } \Omega^\varepsilon, \tag{14a}$$

$$\nabla \cdot \big((\phi^\varepsilon + \delta)\mathbf{q}^\varepsilon\big) = 0 \qquad \text{in } \Omega^\varepsilon, \tag{14b}$$

$$\begin{aligned} \varepsilon^2 \rho_f \Big(\partial_t \big((\phi^\varepsilon + \delta)\mathbf{q}^\varepsilon\big) - \frac{1}{2}\mathbf{q}^\varepsilon \partial_t \phi^\varepsilon + \nabla \cdot \big((\phi^\varepsilon + \delta)\mathbf{q}^\varepsilon \otimes \mathbf{q}^\varepsilon\big)\Big) + (\phi^\varepsilon + \delta)\nabla p^\varepsilon \\ = \varepsilon^2 \mu_f (\phi^\varepsilon + \delta)\nabla^2\big((\phi^\varepsilon + \delta)\mathbf{q}^\varepsilon\big) - \frac{K}{\lambda}\frac{(1-\phi^\varepsilon)n}{\phi^\varepsilon + n}\mathbf{q}^\varepsilon \qquad \text{in } \Omega^\varepsilon, \end{aligned} \tag{14c}$$

$$\partial_t\big((\phi^\varepsilon + \delta)(u^\varepsilon - u^*)\big) + \nabla \cdot \big((\phi^\varepsilon + \delta)\mathbf{q}^\varepsilon u^\varepsilon\big) = D\nabla \cdot \big((\phi^\varepsilon + \delta)\nabla u^\varepsilon\big) \qquad \text{in } \Omega^\varepsilon, \tag{14d}$$

$$\nabla \phi^\varepsilon \cdot \mathbf{n}^\varepsilon = 0 \qquad \text{on } \Gamma^\varepsilon, \tag{14e}$$

$$(\phi^\varepsilon + \delta)\nabla u^\varepsilon \cdot \mathbf{n}^\varepsilon = 0 \qquad \text{on } \Gamma^\varepsilon, \tag{14f}$$

$$\mathbf{q}^\varepsilon = \mathbf{0} \qquad \text{on } \Gamma^\varepsilon. \tag{14g}$$

Remark 3. *Note that the analysis below remains unchanged if $\delta = 0$, when clogging is not considered. In other words, including an ε-independent regularization parameter δ does not affect the upscaling. The presence of $\delta > 0$ ensures that the resulting model is not degenerate, which is important for the numerical examples.*

4.3 The formal asymptotic expansions

We apply the homogenization ansatz, namely we assume that the unknowns can be written as a series expansion in terms of ε with explicit dependence on the micro- and macro-scale variables. For the phase field ϕ^ε this reads

$$\phi^\varepsilon(t, \mathbf{x}) = \phi_0(t, \mathbf{x}, \mathbf{y}) + \varepsilon\phi_1(t, \mathbf{x}, \mathbf{y}) + \varepsilon^2\phi_2(t, \mathbf{x}, \mathbf{y}) + \dots, \tag{15}$$

where the functions $\phi_i(t, \mathbf{x}, \mathbf{y})$ are Y-periodic in $\mathbf{y}$. Similar expansions are assumed for all the dependent variables. The introduction of the micro-scale variable $\mathbf{y}$ is an important aspect: While the ϕ^ε needs to resolve both the micro scale and macro scale behavior, we assume that the functions in the series expansion can separate between slow variability through $\mathbf{x}$ and fast variability through $\mathbf{y}$. Further, the series expansion allows to capture the dominating behavior in ϕ_0, while lower order behavior is captured through the subsequent terms. Also note that macro-scale $\mathbf{x}$ is defined in the entire (non-perforated) domain $\mathcal{D}$, while $\mathbf{y}$ is defined locally in a pore P.

As $\mathbf{y}$ is a local variable behaving like $\mathbf{y} = \varepsilon^{-1}\mathbf{x}$, the spatial derivatives need to be rewritten accordingly. Hence, for a generic variable v one has

$$\nabla v(\mathbf{x}, \mathbf{y}) = \nabla_{\mathbf{x}} v(\mathbf{x}, \mathbf{y}) + \frac{1}{\varepsilon}\nabla_{\mathbf{y}} v(\mathbf{x}, \mathbf{y}), \tag{16}$$

where $\nabla_{\mathbf{x}}$ and $\nabla_{\mathbf{y}}$ are the gradients w.r.t. $\mathbf{x}$, respectively $\mathbf{y}$. We insert the asymptotic expansions (15) and the rescaled derivatives (16) into the model equations (14), and equate terms of same order with respect to ε to isolate the behavior of the system on different scales. In the regularized equations, the term $\phi_0 + \delta$ will appear frequently and we will use the notation $\phi_0^\delta = \phi_0 + \delta$ in this case. Note that $\phi_0^\delta > 0$.

4.3.1 Phase field equation

Equating the dominating $O(1)$ terms in the phase field equation (14a), gives

$$\lambda^2 \partial_t \phi_0 + \gamma P'(\phi_0) = \gamma\lambda^2 \nabla_{\mathbf{y}}^2 \phi_0 - 4\lambda\phi_0(1-\phi_0)\frac{1}{u^*} f(u_0).$$

The dominating term of the corresponding boundary condition (14e) gives $\nabla_{\mathbf{y}}\phi_0 \cdot \mathbf{n}_P = 0$. Observe that the above equation is similar to the original (14a), but involves only spatial derivatives w.r.t. $\mathbf{y}$. Although ϕ_0 still depends on $\mathbf{x}$, $\mathbf{x}$ only appears as a parameter as no derivatives w.r.t. $\mathbf{x}$ are involved. Recalling the Y-periodicity in $\mathbf{y}$, ϕ_0 solves the following *cell problem* for the phase field:

$$\begin{aligned} \lambda^2\partial_t\phi_0 + \gamma P'(\phi_0) = \gamma\lambda^2\nabla_{\mathbf{y}}^2\phi_0 - 4\lambda\phi_0(1-\phi_0)\frac{1}{u^*}f(u_0) \qquad & \text{in } P, \\ \nabla_{\mathbf{y}}\phi_0 \cdot \mathbf{n}_P = 0 \qquad & \text{on } \Gamma_P, \\ \text{Periodicity in } \mathbf{y} \qquad & \text{across } \partial Y. \end{aligned} \tag{17}$$

These cell problem are defined for each macro scale $\mathbf{x}$, meaning thus for each pore as in Figure 3. However, the cell problems are decoupled locally due to the periodicity requirement.

4.3.2 Mass conservation equation

The dominating $O(\varepsilon^{-1})$ term in (14b) gives

$$\nabla_{\mathbf{y}} \cdot \left(\phi_0^\delta \mathbf{q}_0\right) = 0 \text{ in } P, \tag{18}$$

which will be needed in the derivation for the momentum and ion conservation equations. Next, the $O(1)$ terms provide

$$\nabla_{\mathbf{x}} \cdot \left(\phi_0^\delta \mathbf{q}_0\right) + \nabla_{\mathbf{y}} \cdot \left(\phi_0^\delta \mathbf{q}_1 + \phi_1 \mathbf{q}_0\right) = 0.$$

Integrating w.r.t $\mathbf{y}$ over P, applying the Gauss theorem and the boundary conditions $\mathbf{q}_0 = \mathbf{q}_1 = \mathbf{0}$ on Γ_P together with periodicity, one gets

$$\nabla_{\mathbf{x}} \cdot \left(\overline{\phi_0^\delta \mathbf{q}_0}\right) = 0 \text{ in } \mathcal{D}. \tag{19}$$

The overline-notation indicates a quantity averaged over the micro scale. Formally, one can extend the quantities defined in the pore space P by 0 inside the perforations G, allowing for an average over the entire cell Y. For a scalar variable $v(t,\mathbf{x},\mathbf{y})$ we define $\overline{v}(t,\mathbf{x}) = \frac{1}{|Y|}\int_Y v(t,\mathbf{x},\mathbf{y})d\mathbf{y} = \int_P v(t,\mathbf{x},\mathbf{y})d\mathbf{y}$. Note that $|Y|$, the volume of Y, is 1. In this way, the average of the highest order term of the phase field, $\overline{\phi_0}(t,\mathbf{x})$, will correspond to the porosity at time t at the macro-scale location $\mathbf{x}$.

4.3.3 Momentum conservation equation

The dominating $O(\varepsilon^{-1})$ term in (14c) yields

$$\phi_0^\delta \nabla_{\mathbf{y}} p_0 = \mathbf{0},$$

meaning that $p_0 = p_0(t,\mathbf{x})$ is independent of $\mathbf{y}$. The $O(1)$ terms give

$$\phi_0^\delta(\nabla_{\mathbf{x}} p_0 + \nabla_{\mathbf{y}} p_1) = \mu_f \phi_0^\delta \nabla_{\mathbf{y}}^2\left(\phi_0^\delta \mathbf{q}_0\right) - \frac{K}{\lambda}\frac{(1-\phi_0)n}{\phi_0+n}\mathbf{q}_0. \tag{20}$$

We use the linearity of the equation and determine p_1 and $\mathbf{q}_0$ in terms of (the gradient of) p_0. With $\Pi^j(t,\mathbf{x},\mathbf{y})$ and $\mathbf{w}^j(t,\mathbf{x},\mathbf{y})$ solving the cell problems

$$\begin{aligned} \phi_0^\delta(\mathbf{e}_j + \nabla_{\mathbf{y}}\Pi^j) + \mu_f\phi_0^\delta\nabla_{\mathbf{y}}^2\left(\phi_0^\delta\mathbf{w}^j\right) = \frac{K}{\lambda}\frac{(1-\phi_0)n}{\phi_0+n}\mathbf{w}^j \qquad & \text{in } P, \\ \nabla_{\mathbf{y}} \cdot \left(\phi_0^\delta \mathbf{w}^j\right) = 0 \qquad & \text{in } P, \\ \mathbf{w}^j = \mathbf{0} \qquad & \text{on } \Gamma_P, \\ \text{Periodicity in } \mathbf{y} \text{ across } \partial Y, \qquad & j \in \{1,\dots,\dim\}, \end{aligned} \tag{21}$$

we observe that

$$\begin{aligned} p_1(t,\mathbf{x},\mathbf{y}) &= \sum_{j=1}^{\dim} \Pi^j(t,\mathbf{x},\mathbf{y})\partial_{x_j}p_0(t,\mathbf{x}) \\ \mathbf{q}_0(t,\mathbf{x},\mathbf{y}) &= -\sum_{j=1}^{\dim} \mathbf{w}^j(t,\mathbf{x},\mathbf{y})\partial_{x_j}p_0(t,\mathbf{x}), \end{aligned}$$

now fulfill (18) and (20). The boundary condition for $\mathbf{w}^j$ on Γ_P follows from $\mathbf{q}_0 = \mathbf{0}$ on Γ_P. Note that the cell problem is solved in $\mathbf{y}$ for a fixed $\mathbf{x}$. Hence, as with the phase field cell problem, one can solve for single pores independently.

Multiplying with ϕ_0^δ in the last equality and averaging over Y gives

$$\overline{\phi_0^\delta \mathbf{q}_0} = -\mathcal{K}\nabla_{\mathbf{x}} p_0 \text{ in } \mathcal{D}, \tag{22}$$

where the components of the *permeability tensor* $\mathcal{K}(t, \mathbf{x})$ are given by

$$k_{ij}(t, \mathbf{x}) = \int_P \phi_0^\delta w_i^j d\mathbf{y}, \quad \text{with } i, j \in \{1, \dots, \dim\}.$$

Here, w_i^j are the components of $\mathbf{w}^j$, which are the solutions of the cell problems (21) with the continuous extension $\mathbf{w}^j = \mathbf{0}$ inside the grain.

4.3.4 Ion conservation equation

The dominating $O(\varepsilon^{-2})$ term from the ion conservation equation (14d) and dominating $O(\varepsilon^{-1})$ term from the corresponding boundary condition (14f) give

$$\begin{aligned} \nabla_{\mathbf{y}} \cdot \big(\phi_0^\delta \nabla_{\mathbf{y}} u_0\big) &= 0 && \text{in } P, \\ \phi_0^\delta \nabla_{\mathbf{y}} u_0 \cdot \mathbf{n}_P &= 0 && \text{on } \Gamma_P, \end{aligned}$$

along with periodicity in $\mathbf{y}$. This implies that $u_0 = u_0(t, \mathbf{x})$ is independent of $\mathbf{y}$.

Further, the $O(\varepsilon^{-1})$ terms from (14d) and $O(1)$ terms from (14f) give

$$\begin{aligned} \nabla_{\mathbf{y}} \cdot \big(\phi_0^\delta (\nabla_{\mathbf{x}} u_0 + \nabla_{\mathbf{y}} u_1)\big) &= 0 && \text{in } P, \\ \phi_0^\delta (\nabla_{\mathbf{x}} u_0 + \nabla_{\mathbf{y}} u_1) \cdot \mathbf{n}_P &= 0 && \text{on } \Gamma_P, \end{aligned}$$

where we used (18) for the convective term. We exploit again the linearity of the problem and formulate $u_1(t, \mathbf{x}, \mathbf{y})$ in terms of (the derivatives of) $u_0(t, \mathbf{x})$. We let the weight functions $\omega^j(t, \mathbf{x}, \mathbf{y})$ solve the cell problems

$$\begin{aligned} \nabla_{\mathbf{y}} \cdot \big(\phi_0^\delta (\nabla_{\mathbf{y}} \omega^j + \mathbf{e}_j)\big) &= 0 && \text{in } P, \\ \phi_0^\delta (\nabla_{\mathbf{y}} \omega^j + \mathbf{e}_j) \cdot \mathbf{n}_P &= 0 && \text{on } \Gamma_P, \\ \text{Periodicity in } \mathbf{y} &\text{ across } \partial Y, && j \in \{1, \dots, \dim\}, \end{aligned} \tag{23}$$

As earlier, the cell problems are solved in $\mathbf{y}$ for a fixed $\mathbf{x}$. Then, for an arbitrary $\tilde{u}_1 = \tilde{u}_1(t, \mathbf{x})$ we obtain that

$$u_1(t, \mathbf{x}, \mathbf{y}) = \tilde{u}_1(t, \mathbf{x}) + \sum_{j=1}^{\dim} \omega^j(t, \mathbf{x}, \mathbf{y}) \partial_{x_j} u_0(t, \mathbf{x}).$$

As will follow from below, only $\nabla_{\mathbf{y}} u_1$ will be needed for obtaining the upscaled model, therefore the function $\tilde{u}_1$ plays no role in the upscaling and it is not necessary to specify it.

The $O(1)$ terms from (14d) and $O(\varepsilon)$ terms from (14f) give

$$\begin{aligned} \partial_t\big(\phi_0^\delta (u_0 - u^*)\big) + \nabla_{\mathbf{x}} \cdot \big(\phi_0^\delta \mathbf{q}_0 u_0\big) + \nabla_{\mathbf{y}} \cdot \mathbf{A} & \\ = D\big(\nabla_{\mathbf{y}} \cdot \mathbf{B} + \nabla_{\mathbf{x}} \cdot \big(\phi_0^\delta (\nabla_{\mathbf{x}} u_0 + \nabla_{\mathbf{y}} u_1)\big) && \text{in } \mathcal{D} \times P, \\ \mathbf{B} \cdot \mathbf{n}_P = 0 && \text{on } \Gamma_P. \end{aligned}$$

where $\mathbf{A} = \phi_1 \mathbf{q}_0 u_0 + \phi_0^\delta \mathbf{q}_1 u_0 + \phi_0^\delta \mathbf{q}_0 u_1$ and $\mathbf{B} = \phi_0^\delta \nabla_{\mathbf{x}} u_1 + \phi_0^\delta \nabla_{\mathbf{y}} u_2 + \phi_1 \nabla_{\mathbf{x}} u_0 + \phi_1 \nabla_{\mathbf{y}} u_1$. The above equation contains derivates in both $\mathbf{x}$ and $\mathbf{y}$. To find the upscaled model we integrate in $\mathbf{y}$ over the domain P, apply Gauss' theorem in $\mathbf{y}$, use the boundary condition on Γ_P and the periodicity requirement to remove the $\nabla_{\mathbf{y}} \cdot \mathbf{A}$ and $\nabla_{\mathbf{y}} \cdot \mathbf{B}$ terms. For the velocity terms in $\mathbf{A}$, we also apply the boundary condition (14g), which gives $\mathbf{q}_0 = \mathbf{q}_1 = \mathbf{0}$ on Γ_P. This leads to the upscaled reaction-advection-diffusion equation

$$\partial_t\big(\overline{\phi_0^\delta}(u_0 - u^*)\big) + \nabla_{\mathbf{x}} \cdot \big(\overline{\phi_0^\delta \mathbf{q}_0} u_0\big) = D \nabla_{\mathbf{x}} \cdot (\mathcal{A} \nabla_{\mathbf{x}} u_0) \text{ in } \mathcal{D}. \tag{24}$$

The component of the matrix $\mathcal{A}(t,\mathbf{x})$ are

$$a_{ij}(t,\mathbf{x}) = \int_P \phi_0^\delta(\delta_{ij} + \partial_{y_i}\omega^j)d\mathbf{y}, \qquad \text{with } i,j \in \{1,\dots,\dim\},$$

where ω^j is the solution of the cell problem (23). Hence, the upscaled ion conservation equation (24) is to be solved for $\mathbf{x} \in \mathcal{D}$ only, but receiving information from the microscale $\mathbf{y}$ through the effective diffusion matrix and the effective velocity.

4.4 Summary of upscaled equations

To summarize, the upscaled system of equations consist of the three equations (19), (22) and (24) on the macro scale, for the unknowns $\overline{\phi\mathbf{q}_0}(t,\mathbf{x})$, $p_0(t,\mathbf{x})$ and $u_0(t,\mathbf{x})$. The upscaled system is completed by three supplementary cell problems (17), (21) and (23) to be solved locally in each single pores, providing effective properties for the upscaled system.

The regularization δ was kept throughout the upscaling procedure for consistency. We introduced this regularization for avoiding a degeneracy in the system, which would create difficulties in the numerical implementations. For the upscaled model, these difficulties are encountered in the cell problems. Hence, we only consider ϕ_0^δ in the effective properties and set $\delta = 0$ in (19), (22) and (24). Then, for macro scale $\mathbf{x} \in \mathcal{D}$, and for $t > 0$,

$$\begin{aligned}
\nabla_\mathbf{x} \cdot (\overline{\phi_0\mathbf{q}_0}) &= 0 && \text{in } \mathcal{D},\\
\overline{\phi_0\mathbf{q}_0} &= -\mathcal{K}\nabla_\mathbf{x} p_0 && \text{in } \mathcal{D},\\
\partial_t\big(\overline{\phi_0}(u_0 - u^*)\big) + \nabla_\mathbf{x} \cdot (\overline{\phi_0\mathbf{q}_0}u_0) &= D\nabla_\mathbf{x} \cdot (\mathcal{A}\nabla_\mathbf{x} u_0) && \text{in } \mathcal{D},
\end{aligned}$$

where the phase field $\phi_0(t,\mathbf{x},\mathbf{y})$ is updated locally in each pore by solving

$$\begin{aligned}
\lambda^2\partial_t\phi_0 + \gamma P'(\phi_0) &= \gamma\lambda^2\nabla_\mathbf{y}^2\phi_0 - 4\lambda\phi_0(1-\phi_0)\frac{1}{u^*}f(u_0) && \text{in } P,\\
\nabla_\mathbf{y}\phi_0 \cdot \mathbf{n}_P &= 0 && \text{on } \Gamma_P,
\end{aligned}$$

for all $\mathbf{x} \in \mathcal{D}$ and $t > 0$. The effective matrices $\mathcal{K}(t,\mathbf{x})$ and $\mathcal{A}(t,\mathbf{x})$ are found through

$$\begin{aligned}
k_{ij}(t,\mathbf{x}) &= \int_P \phi_0^\delta w_i^j d\mathbf{y}, \text{ where}\\
\phi_0^\delta(\mathbf{e}_j + \nabla_\mathbf{y}\Pi^j) + \mu_f\phi_0^\delta\nabla_\mathbf{y}^2\big(\phi_0^\delta\mathbf{w}^j\big) &= \frac{K}{\lambda}\frac{(1-\phi_0)n}{\phi_0+n}\mathbf{w}^j && \text{in } P,\\
\nabla_\mathbf{y} \cdot \big(\phi_0^\delta\mathbf{w}^j\big) &= 0 && \text{in } P,\\
\mathbf{w}^j &= \mathbf{0} && \text{on } \Gamma_P,
\end{aligned}$$

and

$$\begin{aligned}
a_{ij}(t,\mathbf{x}) &= \int_P \phi_0^\delta(\delta_{ij} + \partial_{y_i}\omega^j)d\mathbf{y}, \text{ where}\\
\nabla_\mathbf{y} \cdot \big(\phi_0^\delta(\nabla_\mathbf{y}\omega^j + \mathbf{e}_j\big) &= 0 && \text{in } P,\\
\phi_0^\delta(\nabla_\mathbf{y}\omega^j + \mathbf{e}_j) \cdot \mathbf{n}_P &= 0 && \text{on } \Gamma_P,
\end{aligned}$$

for $i,j \in \{1,\dots,\dim\}$. The unknowns $\mathbf{w}^j(t,\mathbf{x},\mathbf{y})$, $\Pi^j(t,\mathbf{x},\mathbf{y})$ and $\omega^j(t,\mathbf{x},\mathbf{y})$ fulfill periodicity requirements in $\mathbf{y}$ across ∂Y.

5 Numerical experiments

To illustrate the behavior of the upscaled equations and their dependence on the diffuse interface width, we consider two examples: First, we will solve the cell problems for various choices of λ, showing how the effective ion diffusivity and the flow permeability depend on the width of the diffuse interface. Secondly, to illustrate the behavior of the full system of equations, we consider a simplified geometry, namely a thin strip.

5.1 Solutions to cell problems

For sharp-interface models, cell problems for flow and diffusion for moving-boundary problems using a level set formulation have been derived in [8, 27]. A reasonable simplification is to assume that that if the grains are initially circles (or spheres), the reaction rate is uniform inside each pore and the mineral layer will evolve in a radially symmetric manner and the union of the grain and of the mineral remains a circle (or sphere), see [27]. Hence, the level set formulation can be rewritten into an equation for the radius $R(t, \mathbf{x})$ of the solid (grain and mineral), where the cell problems depend on $R(t, \mathbf{x})$ [10, 27]. In the radially symmetric case, the effective ion diffusivity and the permeability will be scalars.

We adopt a similar approach here, by solving the cell problems (21) and (23) to determine the effective permeability and ion diffusivity by assuming that the phase field has a smooth transition (of $O(\lambda)$) at some distance R from the center of the cell. We do not attempt to determine permeability and diffusivity curves as functions of R as in [10, 27] (see e.g. Figure 3 in [27]), but instead choose some values of R and investigate the behavior as we let the diffuse interface width λ vary.

The cell problems (21) and (23) are discretized using a control volume method on a staggered cartesian grid, where the cell problem unknowns ω^j and Π^j are defined in the centers of the control volumes, and the vectors $\mathbf{w}^j$ are at the edges. For fluxes we apply upstream approximation for the convective terms and two-point flux approximation for diffusive terms. The grid is uniform and quadratical with 800 grid cells in each direction, so that we have at least 8 grid cell through the diffuse transition zone for the smallest λ. Note that the size of the non-reactive part G does not affect the resulting values of the effective variables as long G is well within the mineral phase. For all the cell problems we use a regularization of $\delta = 10^{-8}$.

Remark 4. *Specifying a phase field corresponding to a circular mineral with radius R is not straightforward as no analytical expression exist. An approximate phase field can be found by assuming radial symmetry and considering the reaction-free version of* (17) *in polar coordinates. That is, we seek $\phi(t, r)$ solving*

$$\lambda^2 \partial_t \phi + \gamma P'(\phi) = \gamma \lambda^2 \frac{1}{r} \partial_r (r \partial_r \phi). \tag{25}$$

Because of the non-conservative property of the Allen-Cahn equation, a radially symmetric phase field drop will always shrink towards the center due to curvature effects. Using this, we consider the initial condition

$$\phi(t = 0, r) = \frac{1}{1 + \exp(-4(r - R_0)/\lambda)}, \tag{26}$$

where R_0 is larger than the radius R, which is the mineral radius we seek a phase field for. Following from the curvature-driven movement, the mineral will shrink according to the radial Allen-Cahn equation (25)*. The simulation is stopped when the radius of the transition region reaches R, that is when $\phi = 0.5$ at $r = R$. As boundary conditions we apply $\phi = 0$ at $r = 0$ and $\phi = 1$ at $r = 1$. It could be tempting to directly specify* (26) *with $R_0 = R$ as the phase field, but this would not fulfill the steady-state version of* (25)*. Although* (26) *has similar structure as* (12)*, which is the solution of the one-dimensional steady-state version of the Allen-Cahn equation, this finding cannot be extended to the radially symmetric case due to the structure of the Laplace operator in polar coordinates. This also means that the initial condition* (26) *is only an approximate initial condition.*

5.1.1 Permeability

For the cell problem (21) providing the permeability we consider mineral radii of $R = 0.2,\ 0.3,\ 0.4$. The corresponding permeability values for these mineral radii are $\mathcal{K} = 0.0328,\ 0.0109,\ 0.0018$, respectively [10]. The applied values of λ in (26) will be $\lambda = 0.05,\ 0.04,\ 0.03,\ 0.02,\ 0.01,\ 0.0075,\ 0.005$. In Figure 4, the phase field permeability values are compared to the permeability values resulting from the corresponding sharp interface models. It becomes clear that the phase field permeability values are approaching the ones for the sharp interface models as the values of λ are decreasing. However, the relative errors are large, and are for $\lambda = 0.01$ equal to 5%, 7% and 15% for $R = 0.2,\ 0.3,\ 0.4$, respectively. These deviations can be explained by the fact that flow takes place in the diffuse transition zone, which enhances the flow through the entire cell, and hence overestimates the permeability. This effect is diminished when the parameter K in the phase field cell problem (21) is increased, but larger values of K could also lead to an underestimation of the permeability

if λ is large. For the results in Figure 4, $K = 25$ was used. Hence, finding a good choice for the interpolation function $g(\phi, \lambda)$ in (5c) is essential in the numerical implementation.

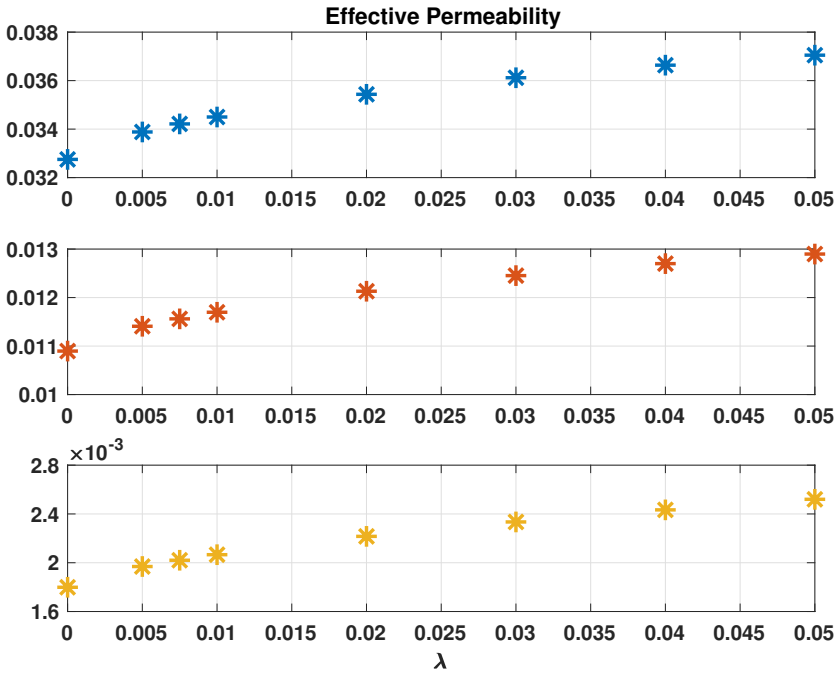

Figure 4: Permeability values for $R = 0.2$ (top), $R = 0.3$ (middle) and $R = 0.4$ (bottom), for various values of λ. The sharp interface values are plotted at $\lambda = 0$.

5.1.2 Effective ion diffusivity

For the effective diffusivity cell problem (23) we consider the same values for R and λ. The effective diffusivities for the sharp-interface model are, for these three values of R, $\mathcal{A} = 0.7767,\ 0.5585,\ 0.3221$, respectively. These values have been found by solving the corresponding sharp-interface cell problems for the diffusion tensor, whose formulation can be found e.g. in [27], using the PDE toolbox in Matlab on recursively finer grids until four digits of accuracy are obtained. The phase field effective diffusion values are compared to the corresponding sharp interface effective diffusion values in Figure 5. Although the phase field values seemingly converge towards a slightly different value than the value provided by the sharp interface model, it is worth noting that the relative errors are rather small ($< 0.3\%$ in all cases), hence the effective diffusion tensors are well approximated even for large values of λ. Note that when defining the transition zone to being where $\phi = 0.5$, leads to a slightly over-estimated size of the grain as the transition zone spreads out radially, which can explain why the diffusion values approaches a slightly too low value. For example, for $R = 0.3$ the true porosity is 0.7173, while the phase field found in Remark 4 with $R = 0.3$ and $\lambda = 0.01$ gives a porosity of 0.7171. Other potential sources of errors would be difference in numerical solvers between the diffuse and sharp-interface discretizations.

5.2 Flow through a thin strip

A simple but instructive test case is when the general model (14) is formulated in a two-dimensional thin strip, mimicking the flow through a long pore. In this case, the scale separation is defined through the ratio $\varepsilon = \ell/L$ between the width ℓ and the length L of the strip. In the non-dimensional case, the domain of the thin strip is $(x, y) \in (0, 1)^2$ due to different scaling of the transversal coordinate y. Note that y now plays the role of the transversal variable, and not a local one, but is still scaled as $y = \varepsilon^{-1}x$ and represents the direction where rapid changes are occurring.

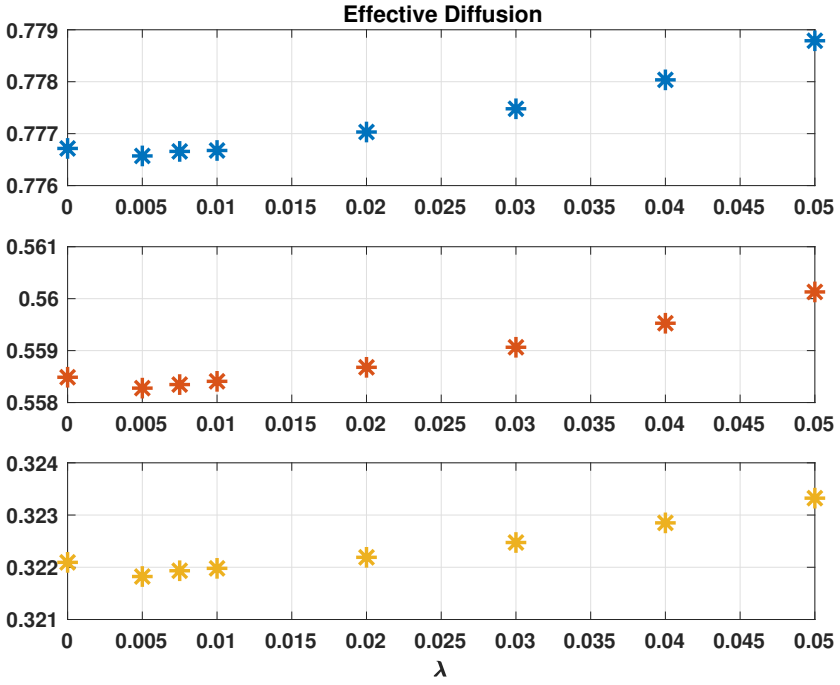

Figure 5: Effective diffusion values for $R = 0.2$ (top), $R = 0.3$ (middle) and $R = 0.4$ (bottom), for various values of λ. The sharp interface values are plotted at $\lambda = 0$.

The model equations for the original two-dimensional strip are (14). The resulting effective model for the thin strip is one-dimensional and is found through asymptotic expansions and transversal averaging of the model equations. Sharp interface formulations for models in a thin strip and considering reactive transport leading to changes in the pore geometry have been formulated and upscaled in [7, 9, 19, 28].

When transversally averaging the model equations, we use a slight reformulation for the phase field equation. Assuming that the mineral is only present as a layer on the upper and lower wall of the strip, and using symmetry across the middle of the strip, the phase field for the lower half of the strip can be approximated by

$$\phi(t, x, y) = \frac{1}{1 + e^{-4(y-d)/\lambda}}, \tag{27}$$

where $d(t, x)$ is the mineral layer width. This form of the phase field is similar to the one used in the matched asymptotic expansions (12), but remains, however, an approximation as zero Neumann conditions at the bottom wall $y = 0$ and symmetry at $y = 1/2$ are not fulfilled. With the unknowns $d(t, x)$, $\overline{\phi}(t, x)$, $u_0(t, x)$, and $\overline{\phi q_0^x}(t, x)$, the upscaled equations obtained by transversal averaging are

$$\partial_t d = f(u_0), \tag{28a}$$

$$\overline{\phi} = 1 + \frac{\lambda}{2} \log\left(1 + e^{-4(0.5-d)/\lambda}\right) - \frac{\lambda}{2} \log\left(1 + e^{4d/\lambda}\right), \tag{28b}$$

$$\overline{\phi q_0^x} = 1, \tag{28c}$$

$$\partial_t(\overline{\phi}(u_0 - u^*)) = -\partial_x(\overline{\phi q_0^x}(u_0 - u^*)) + D\partial_x(\overline{\phi}\partial_x(u_0 - u^*)), \tag{28d}$$

for $x \in (0, 1)$ and $t > 0$. The derivation of these equations can be found in appendix A. Note the absence of a momentum conservation equation, and hence the pressure is not obtained here. Further, we assume that clogging of the pore due to mineral precipitation does not occur, which means that no degeneracy occurs. This allows taking $\delta = 0$, but performing the upscaling for $\delta > 0$ is straightforward.

The original equations (14) are formulated on the scaled strip $(x, y) \in [0, 1]^2$, but using symmetry at $y = 0.5$. Therefore only half of the strip needs to be considered. For both the original system (14) and the transversally

averaged system (28), we design an example including dissolution. We let $u_0(t=0) = u^\varepsilon(t=0) = 0.5$ in the entire domain initially, and inject an ion concentration of $u_0 = u^\varepsilon = 0.25$ at $x = 0$. At the outlet $x = 1$ we assume zero Neumann condition for the ion concentration. The reaction rate is chosen to be $f(u) = u^2/0.5^2 - 1$, corresponding to an equilibrium concentration of $u = 0.5$. Hence, net dissolution will occur when injecting a lower ion concentration. Initially the strip is assumed to be halfway filled with a mineral layer at top and bottom, that is $d(t=0) = 0.25$. The phase field in the original equations is initialized with (27) using $d = 0.25$. Also, we apply zero Neumann condition for the phase field at both inlet and outlet. The original model (14) is initiated with constant pressure and zero velocity. In the upscaled system (28), the inlet condition $\overline{\phi q_0^x} = 1$ also gives the flow through the strip. For the original equations (14), the inlet condition for the along-strip component of the flow rate $\mathbf{q}^\varepsilon$, $q^{\varepsilon,x}$, is formulated using a time-dependent parabolic profile such that $q_x^\varepsilon = 0$ at $y = d(t,0)$, $\partial_y q^{\varepsilon,x} = 0$ at the symmetry line $y = 0.5$, and $\overline{\phi^\varepsilon q^{\varepsilon,x}} = 1$ is fulfilled. The outlet condition for pressure is zero Neumann condition.

The following (non-dimensional) constants have been used in the simulations:

$$D = 1, \quad u^* = 1, \quad \gamma = 0.0075, \quad K = 25, \quad \rho_f = 1, \quad \mu_f = 1,$$

The value of γ is chosen small to ensure low surface curvature effects, while the value of K is chosen large to avoid too much flow in the diffuse transition zone. Also note that the mineral concentration is chosen artificially low so that large changes in the mineral width occurs [28]. We let $\delta = 10^{-6}$ in the original model (14) for all simulations.

Similar to the method in section 5.1, both the original equations (14) and the averaged system (28) are discretized using a control volume method on a staggered cartesian grid where ion concentration, pressure and phase field are defined in the centers of the control volumes, and the velocities across the edges. We apply upstream approximation for the convective terms and two-point flux approximation for diffusive terms. For the original equations rectangular grids are used, where the resolution in the transversal direction is fine enough to resolve the diffuse transition zone properly. For time stepping Euler backward is used for both models. The resulting nonlinear systems of equations are solved using Newton iterations in each time step, with the previous time step as initial guess.

5.2.1 Comparison to sharp interface formulation

For the upscaled system of equations (28), we can compare the obtained solution with similar upscaled models based on a sharp interface formulation, such as the ones found in [7, 28]. Discretizing the sharp interface model with same method, and choosing same initial and boundary conditions, we can investigate the effect of the diffuse interface λ on the model variables.

The are some minor differences in ion concentration u_0, and accordingly in the value of mineral width d as the reaction rate depends on u_0. Figure 6 shows the ion concentrations in the sharp interface model and in the phase field model for various values of λ at $t = 0.5$. For smaller values of λ, the ion concentration approaches the values found through the sharp interface model. The differences in values for the mineral width are small (largest absolute difference for $\lambda = 0.05$ is 0.003).

5.2.2 Comparison to original two-dimensional formulation

We can also check the quality of the upscaling procedure; namely, whether the transversal averages of the output from the original equations (14) approaches the model output found by the upscaled model (28) as ε approaches zero. For this comparison we fix a value of λ and let ε vary. For simplicity we consider $\lambda = 0.05,\ 0.01$, and $\varepsilon = 0.1,\ 0.05,\ 0.025,\ 0.01,\ 0.005$, where the latter corresponds to a strip that is 200 times longer than its width. A typical snapshot from a simulation, with $\lambda = 0.05$ and $\varepsilon = 0.1$ is seen in Figure 7. Even for such a "large" value of ε, the derivatives with respect to y of e.g. ion concentration, is practically zero. The flow field is found through solving Navier-Stokes, and the along-strip component shows a parabola-like profile as expected for this regime. Some flow inside the diffuse interface can be seen.

By vertically averaging the results from the original equations (14) and comparing to the results from the already upscaled model (28), we find in general good correspondence. There is little variability in the transversal direction for ion concentration already for relatively large values of ε, as illustrated in Figure 7 for $\varepsilon = 0.1$. Hence, the averaged ion concentration does not deviate much when decreasing ε. However, some difference is

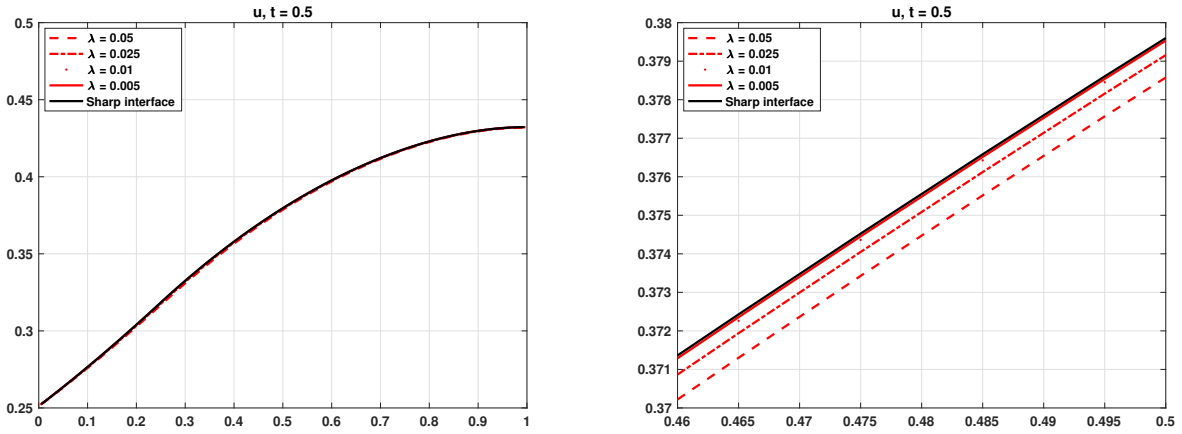

Figure 6: Ion concentration inside thin strip at $t = 0.5$. Right figure shows zoomed in view near the middle of the strip, where the largest differences between the model runs are found.

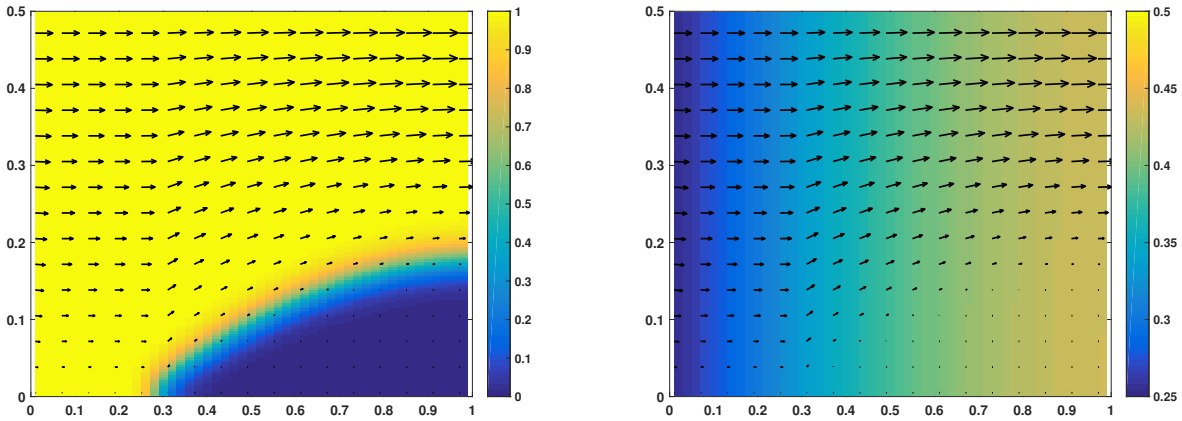

Figure 7: Phase field (left) and ion concentration (right) in thin strip at $t = 0.5$. Note that the y-axis is scaled to fit between 0 and 0.5, but should be between 0 and 0.5ε. Velocity field is given as vector overlay and is mainly along the strip. The transversal component of the velocity field has been scaled with $1/\varepsilon$. For this simulation, $\varepsilon = 0.1$ and $\lambda = 0.05$. The domain was discretized with 50 control volumes in the x-direction and 150 control volumes in the y-direction.

found in the dissolution of the mineral between the two-dimensional model (14) and the upscaled model (28). These differences do not change with smaller ε. The upscaled system of equations uses directly $\partial_t d = f(u)/u^*$, which is equivalent to the reaction rate found in an sharp interface model, while the original phase field equation still has an effect from the interface width λ in the reaction rate. Also, the upscaled model uses an approximated phase field which does not fulfill the boundary conditions at the top and lower boundaries. However, as seen from Figure 8 and Figure 9, the differences in d and u are very small already for $\lambda = 0.05$.

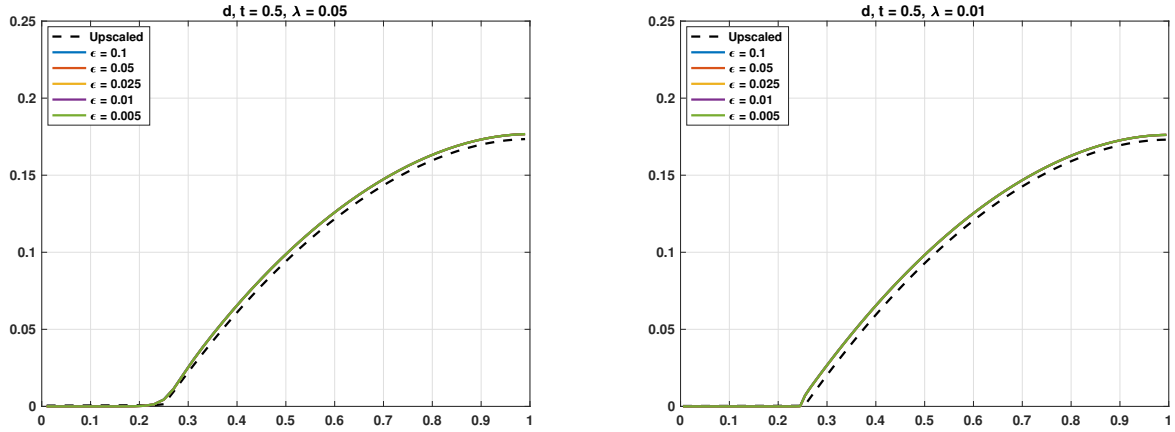

Figure 8: Width of mineral layer $d(t, x)$ inside (the lower half of) the thin strip at $t = 0.5$ for $\lambda = 0.05$ (left) and $\lambda = 0.01$ (right). Note that the colored lines, corresponding to averaged results from the original equations (14), are (almost) on top of each other. The mineral width is found through the phase field by $(0.5 - 0.5\overline{\phi}^{\varepsilon})$.

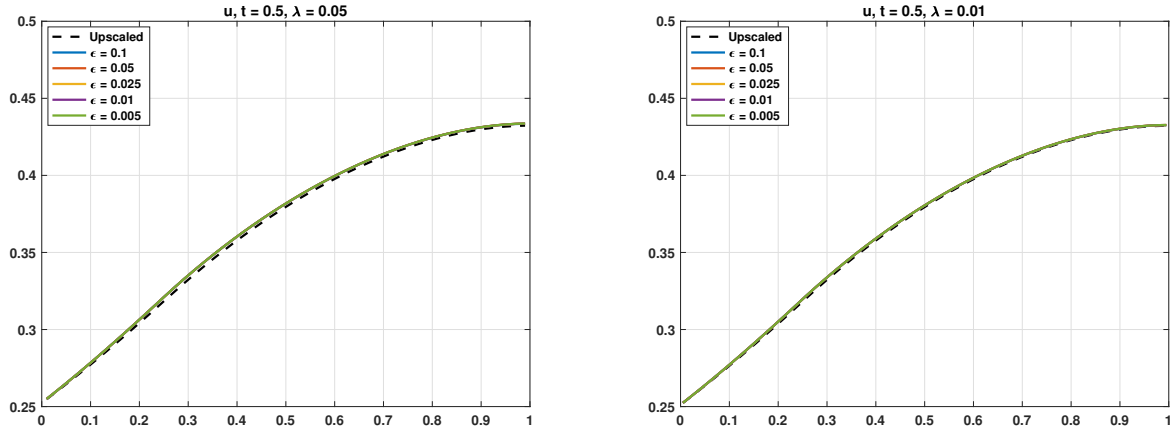

Figure 9: Transversally averaged ion concentration inside thin strip at $t = 0.5$ for $\lambda = 0.05$ (left) and $\lambda = 0.01$ (right). Note that the colored lines, corresponding to averaged results from the original equations (14), are (almost) on top of each other.

6 Conclusions

We have derived a phase field model for reactive transport with mineral precipitation and dissolution. Compared to other modeling approaches involving free boundaries moving due to precipitation and dissolution, the phase

field model has the advantage of being formulated in a fixed domain. The free boundary is then replaced by a diffuse interface region.

The model proposed here extends the one in [22] by incorporating fluid flow. The extension provides mass and momentum conservation by modifying the Navier-Stokes equations, where the phase field variable is incorporated. The momentum conservation equation is further modified by adding a source term to ensure that no flow in the pure mineral phase. Using matched asymptotic expansions, we have shown that the phase field model reduces to the expected sharp interface model when the width of the diffuse interface approaches zero. Hence, the phase field model captures fluid flow and solute transport in the fluid phase, and, as anticipated, no-slip and Rankine-Hugoniot jump conditions at the evolving fluid-mineral interface.

When considering a porous medium, the model proposed here can be seen as a pore scale model. By considering the medium as a periodically perforated one, an upscaled counterpart of the phase field model is obtained by means of homogenization techniques. The resulting effective equations are valid at the Darcy scale. We obtain the cell problems providing the effective ion diffusion are as in [22]. Here we also obtain cell problems for obtaining the effective permeability and porosity. In particular, since the porosity in a cell is the average of the phase field over that cell, the model also provides an equation describing the evolution of the porosity in time, depending on the macro scale location. Numerical experiments show the behavior of the cell problems with respect to the width of the diffuse interface, where the diffusive cell problems provide accurate results for relatively large values of the width of the diffuse interface, while the permeability is prone to being overestimated.

The use of a phase field model instead of a sharp interface formulation avoids some potential numerical pitfalls as there is no need to e.g. solve the level set equation. Using a diffuse interface as replacement of a sharp interface simplifies the development of numerical simulation tools, but also introduces a relaxation which can lead to inaccurate numerical results. As seen from the numerical experiments, the permeability could easily be overestimated or underestimated due to artificial flow in the diffuse transition zone. Hence, using a small value for the width of the diffuse interface is important for obtaining a good representation of the flow at the pore scale or in the cell problems, which in turn puts constraints on how fine the grid has to be near the diffuse interface.

A Thin strip model

We derive here the averaged thin strip model using a phase field formulation, as given in (28). The starting point is the original phase field model for a porous medium (14), but formulated in a thin strip having width ℓ and length L, such that $\varepsilon = \ell/L$ defines the scale separation. Hence, in the non-dimensional setting, the strip has width and length 1, but where derivatives in the y-direction (across the strip) are scaled with $1/\varepsilon$. Hence, for a dummy variable $v(x, y)$ one gets

$$\nabla v(x, y) = \partial_x v \mathbf{i} + \frac{1}{\varepsilon} \partial_y v \mathbf{j},$$

where $\mathbf{i}$ and $\mathbf{j}$ are unit vectors in the along-strip and transversal direction. Due to symmetry we consider only the lower half of the strip. As explained earlier, the phase field approaching value 1 in the fluid part and 0 in the mineral part is given by

$$\phi(t, x, y) = \frac{1}{1 + e^{-4(y-d)/\lambda}}, \tag{29}$$

where $y = d(t, x)$ defines the transition between fluid and mineral where $\phi = 0.5$. This formulation uses $d(t, x)$ as an unknown as in sharp-interface models, but still incorporates a phase field variable that affects the model formulation. However, as ϕ in (29) does not fulfill the zero-Neumann and symmetry boundary conditions, we are making a small error by using this phase field. We here derive the upscaled (transversally averaged) model for the current formulation. As there will be no problems with degeneracy in the equations for the resulting thin strip model, we let $\delta = 0$. It is, of course, possible to do the transversal averaging also with $\delta > 0$, and would only require the phase field ϕ being replaced with $\phi + \delta$ in the ion and mass conservation equations.

A.1 Equation for $d(t,x)$

The equation for $d(t,x)$ is obtained by inserting (29) into the phase field equation (14a) and collect the lowest order terms in ε, $O(\varepsilon^0)$. This gives

$$\lambda^2\partial_t\phi_0 + \gamma P'(\phi_0) = \gamma\lambda^2\partial_y^2\phi_0 - 4\lambda\phi_0(1-\phi_0)\frac{1}{u^*}f(u_0)$$

Inserting (29) for ϕ and using the equalities

$$\partial_t\phi = -\frac{4}{\lambda}\phi(1-\phi)\partial_t d,$$

$$\partial_y^2\phi = \frac{4^2}{\lambda^2}\phi(1-\phi)(1-2\phi),$$

and cancelling equal terms and common factors, results in

$$\partial_t d = \frac{1}{u^*}f(u). \tag{30}$$

Hence, the phase field $\phi(t,x,y)$ is given by (29), where the mineral width $d(t,x)$ follows from (30).

Note that the resulting equation for $d(t,x)$ is the same model equation as used in the sharp interface thin strip formulations as [7, 28]. However, the phase field $\phi(t,x,y)$ will still appear in the upscaled solute transport and flow equations. This allows to illustrate the behavior of the phase field model with respect to λ and ε in a simple setting.

A.2 Equation for the averaged phase field

The transversally averaged phase field will be needed in the upscaled thin strip model. In view of the symmetry, the transversal average of (29) is

$$\overline{\phi} = 2\int_0^{1/2}\frac{1}{1+e^{-4(y-d)/\lambda}}dy = 1 + \frac{\lambda}{2}\log\left(1+e^{-\frac{4}{\lambda}(0.5-d)}\right) - \frac{\lambda}{2}\log\left(1+e^{\frac{4}{\lambda}d}\right).$$

A.3 Equation for mass conservation

The lowest order term arising from the mass conservation equation (14b) yields

$$\partial_y(\phi q_0^y) = 0,$$

which together with the boundary condition (14g) gives that the lowest order transversal velocity component q_0^y is independent of y. The next order provides

$$\partial_x(\phi q_0^x) + \partial_y(\phi q_1^y) = 0,$$

where q_0^x is the lowest order along-strip velocity component and q_1^y is the first order transversal velocity component. This equation is integrated in y from 0 to $1/2$, which together with boundary condition (14g) at $y=0$ and symmetry at $y=1/2$ gives

$$\partial_x(\overline{\phi q_0^x}) = 0.$$

A.4 Equation for average flow rate

Inserting asymptotic expansions into (14c), from the lowest order term one gets

$$\phi\partial_y p_0 = 0,$$

implying that $p_0 = p_0(t,x)$ is independent of y. The logitudinal (along the strip) component of the $O(1)$ terms provide

$$0 = -\phi\partial_x p_0 + \mu_f\phi\partial_y^2(\phi q_0^x) - \frac{K}{\lambda}\frac{(1-\phi)n}{\phi+n}q_0^x.$$

We let $v = \phi q_0^x$ represent the unknown and insert the expression for ϕ, (29) when necessary. Then,

$$\mu_f v'' - \frac{K}{\lambda} \frac{n e^{-4(y-d)/\lambda}(1+e^{-4(y-d)/\lambda})^2}{1+n(1+e^{-4(y-d)/\lambda})} v = \partial_x p_0, \tag{31}$$

where $'$ indicates derivative with respect to y. The variables t and x appearing in d and p are considered parameters. Hence, we have a inhomogeneous, second-order, linear ODE with non-constant coefficients. Finding simple analytical expressions for the solution of v is not straightforward. Instead, the boundary condition $\overline{\phi q_0^x} = 1$ can be used to resolve the flow through the strip together with mass conservation. This means that we will not be able to solve the pressure inside the thin strip.

A.5 Equation for ion concentration

Inserting (29) for ϕ and asymptotic expansion for u^ε into (14d) and equating the lowest order terms yields

$$\partial_y(\phi \partial_y u_0) = 0.$$

Together with the lowest order boundary condition $\phi \partial_y u_0 = 0$ at $y = 0, 1$ and that $\phi > 0$, it follows that

$$u_0 = u_0(t, x).$$

Hence, u_0 is independent of the transversal variable y. Integrating (14d) in y from 0 to $1/2$, and applying boundary conditions (14f) and (14g) on the lower boundary and symmetry conditions on $y = 1/2$, results in

$$\int_0^{1/2} \partial_t(\phi(u^\varepsilon - u^*))dy + \int_0^{1/2} \partial_x(\phi q^{\varepsilon,x}(u^\varepsilon - u^*))dy = D \int_0^{1/2} \partial_x(\phi \partial_x(u^\varepsilon - u^*))dy,$$

where $q^{\varepsilon,x}$ is the along-strip component of the $\mathbf{q}^\varepsilon$. Using the asymptotic expansions and using that u_0 is independent of y leads to

$$\partial_t(\overline{\phi}(u_0 - u^*)) + \partial_x(\overline{\phi q_0^x}(u_0 - u^*)) = D\partial_x(\overline{\phi}\partial_x(u_0 - u^*).$$

Acknowledgments

We would like to thank Profs. Christian Rohde (Stuttgart) and Harald Garcke (Regensburg) for useful discussions on the phase field formulation. The work of the first and the last author was supported by the Research Foundation Flanders (FWO) through the project G0G1316N *DynScale* of the Odysseus program. The second author was funded by the German Research Foundation (DFG) as part of the SFB 1313, Research Project C.02.

References

[1] H. Abels and Y. Liu. Sharp interface limit for a stokes/allen–cahn system. *Archive for Rational Mechanics and Analysis*, 229(1):417–502, Jul 2018.

[2] A. W. Adamson and A. P. Gast. *Physical chemistry of surfaces*. Interscience publishers New York, 1967.

[3] A. Agosti, B. Giovanardi, L. Formaggia, and A. Scotti. A numerical procedure for geochemical compaction in the presence of discontinuous reactions. *Advances in Water Resources*, 94:332 – 344, 2016.

[4] S. M. Allen and J. W. Cahn. A microscopic theory for antiphase boundary motion and its application to antiphase domain coarsening. *Acta Metallurgica*, 27(6):1085 – 1095, 1979.

[5] C Beckermann, H.-J Diepers, I Steinbach, A Karma, and X Tong. Modeling melt convection in phase-field simulations of solidification. *Journal of Computational Physics*, 154(2):468 – 496, 1999.

[6] F. Boyer, C. Lapuerta, S. Minjeaud, B. Piar, and M. Quintard. Cahn–hilliard/navier–stokes model for the simulation of three-phase flows. *Transport in Porous Media*, 82(3):463–483, Apr 2010.

[7] C. Bringedal, I. Berre, I. S. Pop, and F. A. Radu. A model for non-isothermal flow and mineral precipitation and dissolution in a thin strip. *Journal of Computational and Applied Mathematics*, 289:346 – 355, 2015. Sixth International Conference on Advanced Computational Methods in Engineering (ACOMEN 2014).

[8] C. Bringedal, I. Berre, I. S. Pop, and F. A. Radu. Upscaling of non-isothermal reactive porous media flow with changing porosity. *Transport in Porous Media*, 114(2):371–393, 2016.

[9] C. Bringedal, I. Berre, I. S. Pop, and F. A. Radu. Upscaling of nonisothermal reactive porous media flow under dominant peclet number: The effect of changing porosity. *Multiscale Modeling & Simulation*, 14(1):502–533, 2016.

[10] C. Bringedal and K. Kumar. Effective behavior near clogging in upscaled equations for non-isothermal reactive porous media flow. *Transport in Porous Media*, 120(3):553–577, 2017.

[11] G. Caginalp and P. Fife. Dynamics of layered interfaces arising from phase boundaries. *SIAM Journal on Applied Mathematics*, 48(3):506–518, 1988.

[12] J. W. Cahn and J. E. Hilliard. Free energy of a nonuniform system. i. interfacial free energy. *The Journal of Chemical Physics*, 28(2):258–267, 1958.

[13] K. R. Elder, Martin Grant, Nikolas Provatas, and J. M. Kosterlitz. Sharp interface limits of phase-field models. *Phys. Rev. E*, 64:021604, Jul 2001.

[14] H. Garcke, C. Hecht, M. Hinze, and C. Kahle. Numerical approximation of phase field based shape and topology optimization for fluids. *SIAM Journal on Scientific Computing*, 37(4):A1846–A1871, 2015.

[15] D. Jeong and J. Kim. Conservative allen-ĂŞcahn-navier-stokes system for incompressible two-phase fluid flows. *Computers & Fluids*, 156:239 – 246, 2017. Ninth International Conference on Computational Fluid Dynamics (ICCFD9).

[16] P. Knabner, C.J. van Duijn, and S. Hengst. An analysis of crystal dissolution fronts in flows through porous media. part 1: Compatible boundary conditions. *Advances in Water Resources*, 18(3):171 – 185, 1995.

[17] K. Kumar, M. Neuss-Radu, and I. S. Pop. Homogenization of a pore scale model for precipitation and dissolution in porous media. *IMA Journal of Applied Mathematics*, 81(5):877–897, 2016.

[18] K. Kumar, I. Pop, and F. Radu. Convergence analysis of mixed numerical schemes for reactive flow in a porous medium. *SIAM Journal on Numerical Analysis*, 51(4):2283–2308, 2013.

[19] K. Kumar, T. L. van Noorden, and I. S. Pop. Effective dispersion equations for reactive flows involving free boundaries at the microscale. *Multiscale Modeling & Simulation*, 9(1):29–58, 2011.

[20] X. Li, J. Lowengrub, A. Rätz, and A. Voigt. Solving pdes in complex geometries: A diffuse domain approach. *Communications in mathematical sciences*, 7(1):81–107, 2009.

[21] X. Mu, F. Frank, B. Riviere, F. O. Alpak, and W. G. Chapman. Mass-conserved density gradient theory model for nucleation process. *Industrial & Engineering Chemistry Research*, 57(48):16476–16485, 2018.

[22] M. Redeker, C. Rohde, and I. S. Pop. Upscaling of a tri-phase phase-field model for precipitation in porous media. *IMA Journal of Applied Mathematics*, 81(5):898–939, 2016.

[23] F. Schlögl. Chemical reaction models for non-equilibrium phase transitions. *Zeitschrift für Physik*, 253(2):147–161, Apr 1972.

[24] R. Schulz, N. Ray, F. Frank, H. S. Mahato, and P. Knabner. Strong solvability up to clogging of an effective diffusion-precipitation model in an evolving porous medium. *European Journal of Applied Mathematics*, 28(2):179–207, 2017.

[25] C. van Duijn and I. S. Pop. Crystal dissolution and precipitation in porous media: Pore scale analysis. *Journal für die reine und angewandte Mathematik*, 577:171–121, 2004.

[26] C.J. van Duijn and P. Knabner. Travelling wave behaviour of crystal dissolution in porous media flow. *European Journal of Applied Mathematics*, 8(1):49–72, 1997.

[27] T. L. van Noorden. Crystal precipitation and dissolution in a porous medium: Effective equations and numerical experiments. *Multiscale Modeling & Simulation*, 7(3):1220–1236, 2009.

[28] T. L. van Noorden. Crystal precipitation and dissolution in a thin strip. *European Journal of Applied Mathematics*, 20(1):69–91, 2009.

[29] T. L. van Noorden and C. Eck. Phase field approximation of a kinetic moving-boundary problem modelling dissolution and precipitation. *Interfaces and Free Boundaries*, 13(1):29–55, 2011.

[30] T. L. van Noorden and I. S. Pop. A stefan problem modelling crystal dissolution and precipitation. *IMA Journal of Applied Mathematics*, 73(2):393–411, 2008.

[31] T. L. van Noorden, I. S. Pop, and M Röger. Crystal dissolution and precipitation in porous media: L1-contraction and uniqueness. In *Discrete Contin. Dyn. Syst.,(Dynamical Systems and Differential Equations. Proceedings of the 6th AIMS International Conference, suppl.)*, pages 1013–1020. Citeseer, 2007.

[32] Z. Xu and P. Meakin. Phase-field modeling of solute precipitation and dissolution. *The Journal of Chemical Physics*, 129(1):014705, 2008.

UHasselt Computational Mathematics Preprint Series

2019

UP-19-01 *Carina Bringedal, Lars von Wolff, and Iuliu Sorin Pop*, **Phase field modeling of precipitation and dissolution processes in porous media: Upscaling and numerical experiments**, 2019

2018

UP-18-09 *David Landa-Marbán, Gunhild Bødtker, Kundan Kumar, Iuliu Sorin Pop, Florin Adrian Radu*, **An upscaled model for permeable biofilm in a thin channel and tube**, 2018

UP-18-08 *Vo Anh Khoa, Le Thi Phuong Ngoc, Nguyen Thanh Long*, **Existence, blow-up and exponential decay of solutions for a porous-elastic system with damping and source terms**, 2018

UP-18-07 *Vo Anh Khoa, Tran The Hung, Daniel Lesnic*, **Uniqueness result for an age-dependent reaction-diffusion problem**, 2018

UP-18-06 *Koondanibha Mitra, Iuliu Sorin Pop*, **A modified L-Scheme to solve nonlinear diffusion problems**, 2018

UP-18-05 *David Landa-Marban, Na Liu, Iuliu Sorin Pop, Kundan Kumar, Per Pettersson, Gunhild Bodtker, Tormod Skauge, Florin A. Radu*, **A pore-scale model for permeable biofilm: numerical simulations and laboratory experiments**, 2018

UP-18-04 *Florian List, Kundan Kumar, Iuliu Sorin Pop and Florin A. Radu*, **Rigorous upscaling of unsaturated flow in fractured porous media**, 2018

UP-18-03 *Koondanibha Mitra, Hans van Duijn*, **Wetting fronts in unsaturated porous media: the combined case of hysteresis and dynamic capillary**, 2018

UP-18-02 *Xiulei Cao, Koondanibha Mitra*, **Error estimates for a mixed finite element discretization of a two-phase porous media flow model with dynamic capillarity**, 2018

UP-18-01 *Klaus Kaiser, Jonas Zeifang, Jochen Schütz, Andrea Beck and Claus-Dieter Munz*, **Comparison of different splitting techniques for the isentropic Euler equations**, 2018

2017

UP-17-12 *Carina Bringedal, Tor Eldevik, Øystein Skagseth and Michael A. Spall*, **Structure and forcing of observed exchanges across the Greenland-Scotland Ridge**, 2017

UP-17-11 *Jakub Wiktor Both, Kundan Kumar, Jan Martin Nordbotten, Iuliu Sorin Pop and Florin Adrian Radu*, **Linear iterative schemes for doubly degenerate parabolic equations**, 2017

UP-17-10 *Carina Bringedal and Kundan Kumar*, **Effective behavior near clogging in upscaled equations for non-isothermal reactive porous media flow**, 2017

UP-17-09 *Alexander Jaust, Balthasar Reuter, Vadym Aizinger, Jochen Schütz and Peter Knabner*, **FESTUNG: A MATLAB / GNU Octave toolbox for the discontinuous Galerkin method. Part III: Hybridized discontinuous Galerkin (HDG) formulation**, 2017

UP-17-08 *David Seus, Koondanibha Mitra, Iuliu Sorin Pop, Florin Adrian Radu and Christian Rohde*, **A linear domain decomposition method for partially saturated flow in porous media**, 2017

UP-17-07 *Klaus Kaiser and Jochen Schütz*, **Asymptotic Error Analysis of an IMEX Runge-Kutta method**, 2017

UP-17-06 *Hans van Duijn, Koondanibha Mitra and Iuliu Sorin Pop*, **Travelling wave solutions for the Richards equation incorporating non-equilibrium effects in the capillarity pressure**, 2017

UP-17-05 *Hans van Duijn and Koondanibha Mitra*, **Hysteresis and Horizontal Redistribution in Porous Media**, 2017

UP-17-04 *Jonas Zeifang, Klaus Kaiser, Andrea Beck, Jochen Schütz and Claus-Dieter Munz*, **Efficient high-order discontinuous Galerkin computations of low Mach number flows**, 2017

UP-17-03 *Maikel Bosschaert, Sebastiaan Janssens and Yuri Kuznetsov*, **Switching to nonhyperbolic cycles from codim-2 bifurcations of equilibria in DDEs**, 2017

UP-17-02 *Jochen Schütz, David C. Seal and Alexander Jaust*, **Implicit multiderivative collocation solvers for linear partial differential equations with discontinuous Galerkin spatial discretizations**, 2017

UP-17-01 *Alexander Jaust and Jochen Schütz*, **General linear methods for time-dependent PDEs**, 2017

2016

UP-16-06 *Klaus Kaiser and Jochen Schütz*, **A high-order method for weakly compressible flows**, 2016

UP-16-05 *Stefan Karpinski, Iuliu Sorin Pop, Florin A. Radu*, **A hierarchical scale separation approach for the hybridized discontinuous Galerkin method**, 2016

UP-16-04 *Florin A. Radu, Kundan Kumar, Jan Martin Nordbotten, Iuliu Sorin Pop*, **Analysis of a linearization scheme for an interior penalty discontinuous Galerkin method for two phase flow in porous media with dynamic capillarity effects** , 2016

UP-16-03 *Sergey Alyaev, Eirik Keilegavlen, Jan Martin Nordbotten, Iuliu Sorin Pop*, **Fractal structures in freezing brine**, 2016

UP-16-02 *Klaus Kaiser, Jochen Schütz, Ruth Schöbel and Sebastian Noelle*, **A new stable splitting for the isentropic Euler equations**, 2016

UP-16-01 *Jochen Schütz and Vadym Aizinger*, **A hierarchical scale separation approach for the hybridized discontinuous Galerkin method**, 2016